

People's Democratic Republic of Algeria
Ministry of Higher Education and Scientific Research
University M'Hamed BOUGARA – Boumerdes



Institute of Electrical and Electronic Engineering
Department of Power and Control

Final Year Project Report Presented in Partial Fulfilment of
the Requirements for the Degree of

MASTER

In Power Engineering

Option: Power Engineering

Title:

**Control of Stand-Alone PV System Under
Non-Uniform Irradiance**

Presented by:

- **ZERROUKI NIHAL**
- **DAHMAN GHENIMA**

Supervisor:

Dr.Kheldoun Aissa

Registration Number:/2019

Abstract

Renewable energy sources play vital role in power generation, research in this area has grown rapidly in the last few years and the society is now aware of the harmful effects of fossil fuel on the environment and with the increased cost of fuel production. It is very important to look for alternative efficient, clean and cheap energy sources. Solar energy is usually considered as one of the most promising renewable energy sources.

The power generation from the photovoltaic panels is subjected to varying environmental conditions such as temperature and irradiance which lead to a varying conversion efficiency. This necessitates an optimum use of the incident solar radiation. Since a PV unit supplies maximum electrical power only at a certain operating point, Maximum Power Point Trackers (MPPT) were developed to seek this optimal operation under changing light and load conditions. These methods would ensure an efficient and more reliable energy source.

This project is intended to simulate and implement a GMPPT for stand-alone PV system in order to provide a fast, efficient tracking solution. PV generators develop a very complex power versus voltage characteristics. That is, under non-uniform isolation, the PV generators exhibit a curve with many power peaks. Identifying the appropriate peak during the operation is the goal of the MPPT for Proper and efficient operation of the PV system, therefore three algorithms are to be studied during this project which are the incremental conductance algorithm one of the most commonly used technique, the golden section search GSS algorithm and the particle swarm optimisation PSO algorithm, a comparison would be done by implementing the algorithms using MATLAB/SIMULINK to find the best MPPT algorithm that converges rapidly avoiding errors and obtaining the best efficiency.

Dedication

I dedicate this thesis to my parents, my father AHMED, who always had confidence in me and offered me encouragement and support in all my endeavours. My wonderful mother HAFIDHA, with her endless love she taught me to persevere and prepared me to face any challenges. She was constant source of inspiration to my life who gave me strength and support, her presence that urge me to strive to achieve my goals in life. And I will always make sure you witness my success.

My littles brothers Abd-elghani, Abd-errahman, my sisters Amina, F. Zahra and Brothers in law and their children, beside the angel INES

Zerrouki Nihal

This work is dedicated first to my mother , the light that guides me through every step in my life and whom without her support I wouldn't be what I am today ,then to my family members from my grand-parents, aunts and uncles to brothers and sisters in law who encouraged me during my whole journey at inelec and kept me away from giving up , and finally to my friends who care about my success and whom I consider as sisters, Sabrina & Lynda

Dahman Ghenima

Acknowledgement

We would first like to express our gratitude to our thesis advisor **Dr KHELDOUN AISSA** for his constant support throughout the achievement of this work, the door to his office was always open whenever we ran into a trouble spot or had a question about our research or realisation of the project. He consistently allowed this project to be our own work, but steered us in the right direction whenever he thought we needed it.

We would also like to thank our teachers of the institute IGEE for their help especially **Dr METIDJI BRAHIM** who played a major role in our implementation by providing the necessary resources and guiding us in addition to **Dr AMMAR ABDELKARIM** for their efforts.

Finally, we must express our very profound gratitude to our parents for providing us with unfailing support and continuous encouragement throughout our years of study and through the process of researching and writing this thesis. This accomplishment would not have been possible without them. Thank you.

Table of contents

| | |
|---------------------------|------|
| Abstract..... | I |
| Dedication..... | IV |
| Acknowledgment..... | III |
| Table of contents..... | IV |
| List of Figures | VII |
| List of Tables | XII |
| List of abbreviation..... | XIII |

General Introduction..... 1

Chapter 1: Modelling of Photovoltaic System Parameters..... 3

| | |
|---|----|
| 1.1 Introduction..... | 3 |
| 1.2 PV principle..... | 3 |
| 1.2.1-Semiconductor physic..... | 4 |
| 1.3 PV levels..... | 6 |
| 1.3.1- PV cell..... | 6 |
| 1.3.2- PV module..... | 9 |
| 1.3.3- PV array..... | 10 |
| 1.4 Non-Linear characteristics of PV's | 11 |
| 1.5 Characteristics of the PV system under partial shading..... | 13 |
| 1.6 Conclusion..... | 17 |

Chapter 2: Maximum power point tracking (MPPT) 18

| | |
|-----------------------|----|
| 2.1 Introduction..... | 18 |
|-----------------------|----|

| | |
|--|-----------|
| 2.2 Maximum power point tracking..... | 18 |
| 2.3 MPPT components..... | 19 |
| 2.3.1- Controller..... | 19 |
| 2.3.2- DC/DC Converter..... | 19 |
| 2.3.3- Pulse Width Modulation Unit (PWM)..... | 21 |
| 2.4 MPPT Algorithms..... | 21 |
| 2.4.1- Incremental Conductance..... | 21 |
| 2.4.2- Golden Section Search..... | 23 |
| 2.4.3- Particle Swarm Optimisation..... | 25 |
| 2.5 Conclusion..... | 29 |
| Chapter 3: Simulation and Results..... | 30 |
| 3.1 Introduction..... | 30 |
| 3.2 Presentation of the system without MPPT Controller..... | 30 |
| 3.2.1- PV module characteristics (single- multiple) under uniform irradiance..... | 30 |
| 3.2.2- PV module characteristics (single- multiple) under partial Shading condition..... | 32 |
| 3.3 Presentation of the system with MPPT Controller..... | 33 |
| 3.3.1- Non inverting buck-boost converter (DC-DC converter)... | 33 |
| 3.3.2- Incremental Conductance..... | 36 |
| 3.3.2.1- Incremental Conductance MPPT for a Single Module- under uniform conditions..... | 36 |
| 3.3.2.2- Incremental Conductance MPPT for Five Series Modules- under uniform conditions..... | 39 |
| 3.3.2.3- Incremental Conductance MPPT for Five Series Modules- under shading conditions..... | 42 |
| 3.3.3- Golden Section Search GSS..... | 44 |
| 3.3.3.1- GSS MPPT for a Single Module- under uniform conditions..... | 44 |
| 3.3.3.2- GSS MPPT for FiveSeries Modules- under uniform conditions..... | 46 |

| | |
|--|-----------|
| 3.3.3.3- GSS MPPT for Five Series Modules- under shading conditions..... | 48 |
| 3.3.4- Particle Swarm Optimisation..... | 50 |
| 3.3.4.1- PSO MPPT for a Single Module- under uniform conditions..... | 50 |
| 3.3.4.2- Incremental Conductance MPPT for Five Series Modules- under uniform conditions..... | 52 |
| 3.3.4.3- Incremental Conductance MPPT for Five Series Modules- under shading conditions..... | 53 |
| 3.4 Conclusion..... | 55 |
| Chapter 4: Implementation and discussion..... | 56 |
| 4.1 Introduction..... | 56 |
| 4.2 Real PV characteristics | 56 |
| 4.3 The Implemented System | 59 |
| 4.3.1- Measurement devices and circuit | 60 |
| 4.3.1.a- Current Sensor..... | 60 |
| 4.3.1.b- Voltage Sensor..... | 60 |
| 4.4 Switching Elements..... | 61 |
| 4.4.1- Gate Drive circuit for MOSFET..... | 61 |
| 4.4.2- Buck-Boost Converter..... | 63 |
| 4.4.3- Overall System..... | 65 |
| 4.5 Conclusion..... | 66 |
| General Conclusion..... | 67 |
| Appendix A | |
| Appendix B | |
| Appendix C | |
| References | |

LIST OF FIGURES

Chapter 1: Modelling of Photovoltaic System Parameters

- Figure 1.1: Electron configuration on different shells of the silicon atom.
- Figure 1.2: Doping of silicon: (a) With pentavalent atom (b) With trivalent atom.
- Figure 1.3: Generation of electron-hole pairs by light.
- Figure 1.4: Photons colliding with the p-n junction diode freeing electrons.
- Figure 1.5: Voltage drop across the two terminals of the diode.
- Figure 1.6: Diagram of PV cell.
- Figure 1.7: Equivalent circuit model for PV cell.
- Figure 1.8: A typical current(I-V) curve for a solar cell for different loads.
- Figure 1.9: Connection of identical PV cells. (a) In series_(b) In parallel.
- Figure 1.10: Effect of temperature changes on I-V curves.
- Figure 1.11: Effect of solar irradiance changes on I-V curves.
- Figure 1.12: Effect of temperature changes on P-V curves.
- Figure 1.13: Effect of solar irradiance changes on P-V curves.
- Figure 1.14: PV system under partially shaded conditions caused by passing cloud.
- Figure 1.15: the connection of bypass and blocking diodes to a PV array.
- Figure 1.16: Power-voltage curve of each string under partial shading.
- Figure 1.17: Power-voltage curve of a PV array under partial shading with and without bypass diode.

Chapter 2: Maximum power point tracking (MPPT)

- Figure 2.1: MPPT tracking system.
- Figure 2.2: Proposed DC-DC buck-boost converter.

Figure 2.3: Sample switching pulse.

Figure 2.4: Flowchart of the IC method with direct control.

Figure 2.5: Flowchart of the GSS method.

Figure 2.6: Movement of particles in the optimization process.

Figure 2.7: Flowchart of PSO based on GMPPT.

Chapter 3: Simulation and Results

Figure 3.1: Simulink model of a single PV module.

Figure 3.2: P-V and I-V characteristics of a single module.

Figure 3.3: P-V and I-V characteristics of 5 modules in series.

Figure 3.4: Simulink model of 5 modules in series under PS with bypass diodes.

Figure 3.5: I_V and P_V curves of 5 modules in series under PS with bypass diodes.

Figure 3.6: Simulink model of a non-inverting buck boost converter.

Figure 3.7.a: output voltage of a non-inverting buck boost converter.

Figure 3.7.b: Output voltage of a non-inverting buck-boost converter.

Figure 3.8: Simulink model of a PV module using MPPT controllers.

Figure 3.9: Voltage curve of single PV module using incremental conductance MPPT.

Figure 3.10: Current curve of single PV module using incremental conductance MPPT.

Figure 3.11: Power curve of single PV module using incremental conductance MPPT.

Figure 3.12: Overall system of 5 series connected modules with different MPPT controllers.

Figure 3.13: Voltage curve of five PV modules under uniform conditions using incremental conductance MPPT.

Figure 3.14: Current curve of five PV modules under uniform conditions using incremental conductance MPPT.

Figure 3.15: Power curve of five PV modules under uniform conditions using incremental conductance MPPT.

Figure 3.16: Voltage curve of five PV modules under non-uniform conditions using incremental conductance MPPT.

Figure 3.17: Current curve of five PV modules under non-uniform conditions using incremental conductance MPPT.

Figure 3.18: Power curve of five PV modules under non-uniform conditions using incremental conductance MPPT.

Figure 3.19: Voltage curve of single PV module under uniform conditions using GSS MPPT.

Figure 3.20: Current curve of single PV module under uniform conditions using GSS MPPT.

Figure 3.21: Power curve of single PV module under uniform conditions using GSS MPPT.

Figure 3.22: Voltage curve of five PV modules under uniform conditions using GSS MPPT.

Figure 3.23: Current curve of five PV modules under uniform conditions using GSS MPPT.

Figure 3.24: Power curve of five PV modules under uniform conditions using GSS MPPT.

Figure 3.25: Voltage curve of five PV modules under partial shading conditions using GSS MPPT.

Figure 3.26: Current curve of five PV modules under partial shading conditions using GSS MPPT.

Figure 3.27: Power curve of five PV modules under partial shading conditions using GSS MPPT.

Figure 3.28: Voltage curve of single PV module under uniform conditions using PSO MPPT.

Figure 3.29: Current curve of single PV module under uniform conditions using PSO MPPT.

Figure 3.30: Power curve of single PV module under uniform conditions using PSO MPPT.

Figure 3.31: Voltage curve of five PV modules under uniform conditions using PSO MPPT.

Figure 3.32: Current curve of five PV modules under uniform conditions using PSO MPPT.

Figure 3.33: Power curve of five PV modules under uniform conditions using PSO MPPT.

Figure 3.34: Voltage curve of five PV modules under partial shading conditions using PSO MPPT.

Figure 3.35: Current curve of five PV modules under partial shading conditions using PSO MPPT.

Figure 3.36: Power curve of five PV modules under partial shading conditions using PSO MPPT.

Chapter 4: Implementation and discussion

Figure 4.1: Overall system, Variable resistor and PVs connections.

Figure 4.2: IV and PV characteristics at 9 am.

Figure 4.3: IV and PV characteristics at 4pm.

Figure 4.4: the LA 55-P connection.

Figure 4.5: the LV 25-P connection.

Figure 4.6: measurement circuit.

Figure 4.7 schematic of the gate driver circuit.

Figure 4.8: Gate driver implementation.

Figure 4.9: DC-DC Buck-Boost converter.

Figure 4.10: Simulink model for setting the buck boost.

Figure 4.11.a: obtained PWM pulses from the DSP by assuming duty cycle

Figure 4.11.b: obtained PWM pulses from the DSP by assuming duty cycle

Figure 4.12: Control circuit.

Figure 4.13: Overall system.

LIST OF TABLES

| | |
|---|----|
| Table 3.1: parameters of STH-215-P..... | 30 |
| Table 3.2: Initialization of parameters for a single module..... | 36 |
| Table 3.3: Irradiance profile under uniform conditions..... | 36 |
| Table 3.4: Initialization parameters for 5 series modules..... | 39 |
| Table 3.5: Irradiance profile under non-uniform conditions for 5 series modules.. | 42 |
| Table 3.6: initialization parameters for a single module..... | 50 |
| Table 3.7: PSO Algorithm constants..... | 50 |
| Table 4.1: Recorded values for I_{pv} and V_{pv} at 9 am..... | 57 |
| Table 4.2: recorded values for I_{pv} and V_{pv} at 4 pm..... | 58 |

LIST OF ABBREVIATIONS

A: diode ideality factor

Eg: band gap energy (EV= electron volt)

ki: Short-circuit temperature/current coefficient

Kv: open-circuit temperature/voltage coefficient

Gr: Nominal irradiance level (W/m²)

G: Nominal irradiance level (W/m²)

Tk: Operating temperature (K)

Tdif = deviation of the operating temperature from the reference temperature (K)

Ns: number of series connected cells

V: Voltage (V)

Voc: open circuit voltage (V)

Vpv: PV output voltage (V)

Vmp: maximum Pv output voltage (V)

I0 : diode Current (A)

Iph: Solar-Generated current (A)

Is: diode saturation current (A)

Irs: reverse saturation current (A)

Isc: short circuit current (A)

Ipv: PV output current (A)

Imp: maximum Pv output current (A)

Vpv: PV output voltage

Vmp: maximum Pv output voltage

Rs: series resistance (Ω)

Rp: parallel resistance (Ω)

InC: incremental conductance

PSO: particle swarm optimisation

GSS: golden section search

MPPT: maximum power point tracking

D: duty cycle

P: power (W)

Pbest: Local best (W)

Gbest: Global best (W)

General Introduction

General Introduction

In our days we became more aware of the need for sustainable management of energy resources and we realized that our current rates of energy consumption cannot be maintained for long using scarce energy sources such as crude oil and natural gas. either due to the fact that they are vanishing or their adverse environmental impact contributing in global warming and pollution. The need for renewable energies became imminent to provide energies which are naturally reproduced, clean and cheap. Renewable energy is the type of energy that comes from resources which are naturally replenished on a human timescale such as the Sun light, wind, tidal and geothermal.

Solar Energy is one of the main sources of renewable energy, it relies on the sun as an infinite accessible fuel source. Solar energy can be used in many developed forms from sophisticated photovoltaic panels which convert the sun light directly to electricity, to more simple application in where heat energy produced from the sun is collected for direct use in heating or even evaporation of liquids to form steam to drive turbines and generating electricity.

Nowadays to produce electricity the most used renewable energy is the solar energy through the mean of photovoltaic panels, which are easy to implement specially in isolated regions. A great deal of research has been conducted in this field over the last few decades in order to optimize this new technology and overcome its drawbacks. Compared with conventional fossil energy sources, small scale stand-alone photovoltaic (PV) systems are the best option for many remote applications around the world, they provide power for hundreds of thousands of installations throughout the world. They, particularly in developing countries where two billion people still do not have access to electricity.

Photovoltaic work on the principle of converting sun light energy (photons) into electricity using semiconductors which have the ability to allow the movement of electrons easily .The major advantages of PV systems are their reliability , long life time, no polluting gases emission , no moving parts and no consumed materials are needed , require no connections to another supplying source , processes are completely

solid state and self-contained. They can be installed and upgraded as modular building blocks; more photovoltaic modules may be added as power demand increases.

The problem faced using PV panels is their high dependency on weather factors such as the temperature and irradiance, where under partial shading the PV cells lose their produced energy as a result the efficiency of the plant decreases, beside that these factors make the PV, I-V characteristics non-linear hence makes the tracking and identification of the maximum power point a difficult task.

Many algorithms were implemented for the purpose of tracking the MPPT of PV systems, some of the conventional ones are the Perturb and observe algorithm and the incremental conductance algorithm whereas the new algorithms work on the principle of artificial intelligence and particle swarm optimisation, the difference between conventional and new algorithms is their efficiency since the conventional algorithms sometimes fail to due to discriminate between local and global maxima.

The objective of the project is to implement a fast, accurate and reliable algorithm which tracks the MPPT, the simulation has been done using design software MATLAB/Simulink. The implemented algorithms were the incremental conductance, GSS and PSO and the hardware prototype was made using a PV generator and DSP microcontroller. The later controls the buck-boost chopper in order to harvest the maximum power from the PV panels.

This thesis consists of four chapters, starting with chapter 1 that presents a general background about PV systems Chapter 2 explains the maximum power point tracking algorithms that are to be implemented. Chapter 3 will include the simulation and framework and the obtained results of the investigated MPPT techniques. Chapter 4 is dedicated to the implementation of the studied PV system. Finally, a conclusion of the work done through this thesis and a discussion about future work are presented at the end of this report.

Chapter One

Modelling of Photovoltaic System

1.1 Introduction

Solar energy is the solar radiation that reaches earth from a source emitter which is the sun, that is multiple billions of years old. Two forms are used to generate electricity, the solar thermal and photovoltaic energy. Solar thermal Plants which work on indirect conversion of solar heat into electricity, by heating water and using this steam to power the turbines of the power generators. And the most used one is Photovoltaic (PV devices) or “solar cells” where Solar energy is directly converted to electricity using semiconductors to provide electricity for remote locations with no connection to the electric grid and devices that dissipate low power such as street lighting, communication systems.

The major disadvantages of solar energy are: The sunlight intensity that is converted into energy depends of many factors such as time of the day and the weather; the power over collector area relation is extremely low,[1].

In this chapter, we will focus on overall backgrounds required to design a photovoltaic system, namely, solar power fundamentals, photovoltaic cells modules arrays, and power conditioning elements.

1.2 PV principle

Photovoltaic works with semiconductor physics. This section demonstrates the physics behind the generation of electricity using solar power. The photovoltaic effect is based on the molecular characteristics of semiconductors.

The silicon is one of the most used semiconductor materials in photovoltaic. It has four valence electrons and a diamond crystal structure, mainly it conducts poorly due to the lack of free electrons in the conduction band of its atoms. If an electron in the valence band was supplied with sufficient energy it would be excited to the conduction band and would be able to move freely within the material.

figure 1.1 shows the electrons configuration on the different shells of a silicon atom in both actual form and simplified one, [1].

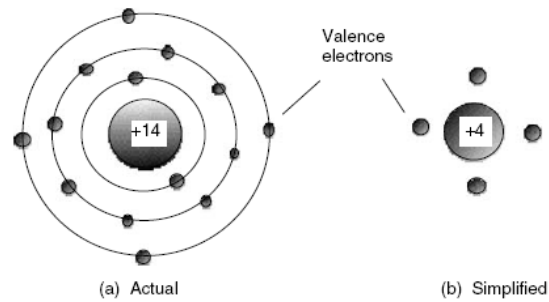


Figure 1.1: Electron configuration on different shells of the silicon atom.

1.2.1 Semiconductor physics:

PV cells consist of layered silicon that is doped¹ with different elements to form a p-n junction. The p-type side will contain positive charges. The n-type side will contain negative charges. This difference of charge forms a region that is charge neutral and acts as a sort of barrier.

Figure 1.2: shows the doping of the silicon semiconductor with trivalent/ pentavalent atom

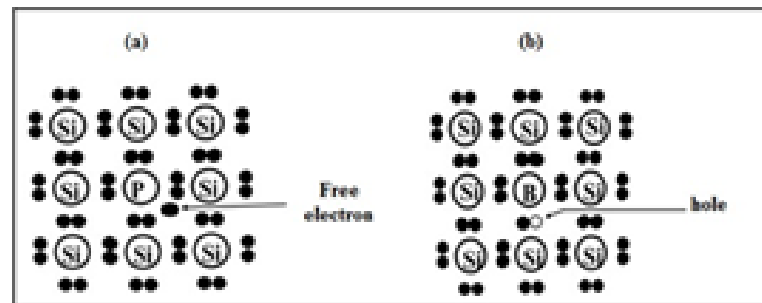


Figure 1.2: Doping of silicon: (a) With pentavalent atom
(b) With trivalent atom.

When the p-n junction is exposed to light, photons with correct frequency will form an electron/hole pair. However, since the p-n junction creates a potential difference, the electrons cannot jump to the other side only the holes can. Thus, the

¹ **doping** is the addition of impurities into a pure semiconductor such as silicon for the purpose of modulating its electrical properties

electrons must exit through the metal connector and flow through the load, to the connector on the other side of the junction. Figure 1.3: shows the generation of electron-hole pair when a photon delivers its energy:

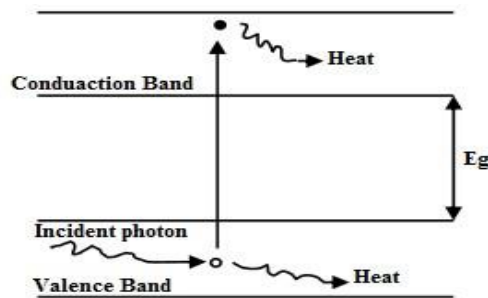


Figure 1.3: Generation of electron-hole pairs by light.

If the photons free an electron in the p-type material near the depletion region It will be carried by the E-field to the n-type material, thus affecting the same process for a hole travelling from and to the opposite sides, creating a current. [1]

Figure 1.4 shows the collision of photons freeing electrons.

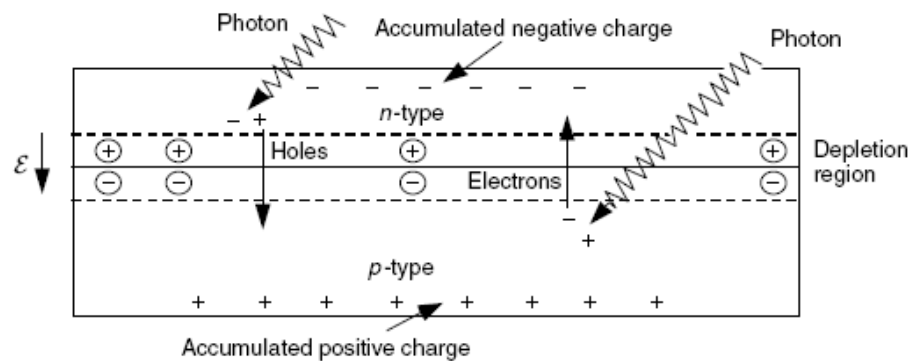


Figure 1.4: Photons colliding with the p-n junction diode freeing electrons.

The connection of the two terminals of the diode with exposure to light will result a voltage drop according to Figure 1.5

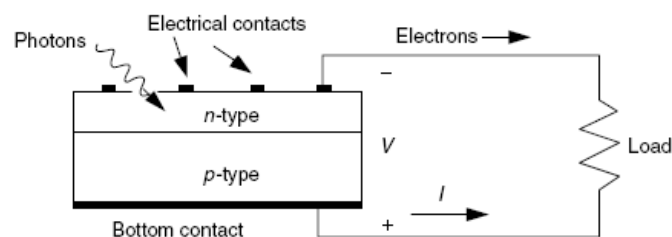


Figure 1.5: Voltage drop across the two terminals of the diode.

1.3 PV levels

1.3.1- PV cell:

The solar cell is the smallest entity that produces electricity, made up of silicone, with a small structure and an absorbing material. Many different solar cells are now available on the market- Some are still under development seeking better efficiency while keeping cost to a minimum. Devices with efficiency exceeding 30% have been demonstrated in the laboratory. However, the efficiency of commercial ones is usually less than half this value. Crystalline silicon cells hold the largest part of the market (higher efficiency and longer life time) but are still expensive. Multi-crystalline material is used more and more to reduce the cost.

- **PV Cell model:**

Solar cells are an array of p-n junction diodes connected together that generate current using photon energy.

Figure 1.6 shows a typical diagram of a PV cell. On the two sides of the cell highly doped layers are formed (Si n- type and SI p+ type) that help in the separation of photons from the centre region.

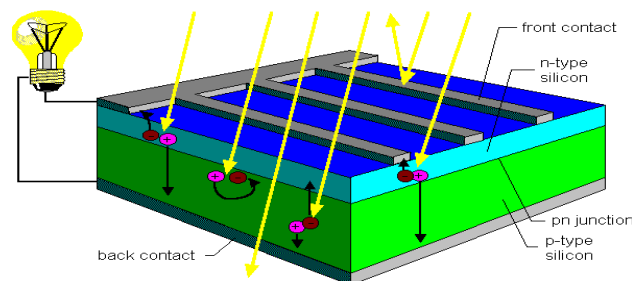


Figure 1.6: Diagram of PV cell.

The single-diode circuitry for a real photovoltaic cell is represented in Figure 1.7 shows the output of photovoltaic systems corresponds directly to solar irradiance and temperature, therefore obtaining the maximum power point should involve the most recent values of these factors. equation 1.1 defines the output current of a pv cell .

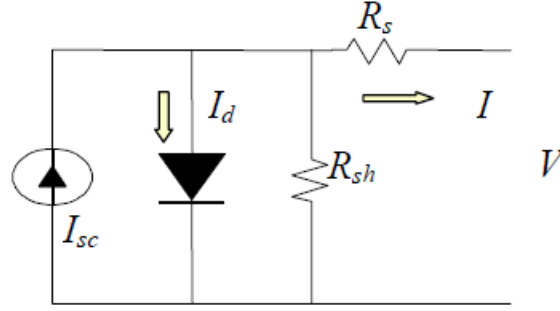


Figure 1.7: Equivalent circuit model for PV cell.[2]

$$I_{pv} = I_{sc} - I_0 \left\{ \exp \left[\frac{q(V + R_s I)}{n K T_k} \right] - 1 \right\} - \frac{V + R_s I}{R_{sh}} \quad (1.1)$$

- **The mathematical model:**

From the equivalent circuit of the PV cell the mathematical model of parameters can be defined [8]. the short circuit current (I_{sc}) and the open circuit voltage (V_{oc}), which are gleaned from the cell manufacturer's data sheet.

By applying Kirchhoff's law on the common node of the current source, diode and resistances, the PV current can be derived by:

$$I_{pv} = I_{sc} - I_d - \left(\frac{V - I_{sc} R_s}{R_{sh}} \right) \quad (1.2)$$

I_{pv} : represents the output current to be fed through the load

I_d : represents the diode current.

I_{sc} : represents the solar-generated current which can be calculated as follow [3,4]:

$$I_{sc}(G) = (I_{scref} + K_i * T_{dif}) \frac{G}{G_r} \quad (1.3)$$

K_i : is the temperature coefficient

T_{dif} : is the difference between ambient temperature and the reference ($T_{dif} = T_k - T_r$)

G and G_r : are the operating and reference irradiances, respectively.

I_{scref} : is reference short circuit current (1000 W/m^2).

Meanwhile, the reverse saturation current (I_{rs}) at a certain reference temperature can be calculated using equation (1.4). [5,6]

$$I_{rs} = \frac{I_{sc}}{\exp\left(\frac{q \cdot E_{oc}}{K_b \cdot A \cdot T_k} - 1\right)} \quad (1.4)$$

A: is the diode ideality factor,

q: is the constant known as the electron charge ($q = 1.602 \times 10^{-19}$ C);

Kb: is the Boltzmann constant.

As stated earlier, I_o is the diode current that will be calculated by the Shockley Equation (1.5) [7]:

$$I_o = I_{o1} \left[\exp\left(\frac{q(V_{pv} + I_{pv} \cdot R_s)}{A \cdot K_b \cdot T_k}\right) - 1 \right] \quad (1.5)$$

In the meantime, the diode saturation current (I_{o1}) fluctuates in accordance with particular environmental changes, and so can be determined by equation (1.6) [4,6]

$$I_{o1} = I_{rs} \left(\frac{T_k}{T_r}\right)^3 \exp\left[\frac{q \cdot E_{g0}}{A \cdot K_b} \left(\frac{T_{dif}}{T_r \cdot T_k}\right)\right] \quad (1.6)$$

E_{g0} : refers to the band gap energy for the silicon E_{g0} is in the range [1.1-1.2 eV]

Finally, we obtain the formula for the PV cell's output current [4]

$$I_{pv} = I_{sc} - I_{o1} \left[\exp\left(\frac{q(V_{pv} + I_{pv} \cdot R_s)}{A \cdot K_b \cdot T_k}\right) - 1 \right] \quad (1.7)$$

R_{sh} : is the parallel resistance which normally has a high resistance and sometimes assumed infinity, due to its slight impression.

R_s : is the series resistance which value cannot be ignored according to its impacts on output power.

Figure 1.8 shows the I-V characteristics of the solar cell, when exposed to the sun light and connected to a load, for a given temperature. Three zones can be

observed: MN region, where the current is nearly constant, PS region in which the voltage is also nearly constant and NP region which contains the maximum power point A

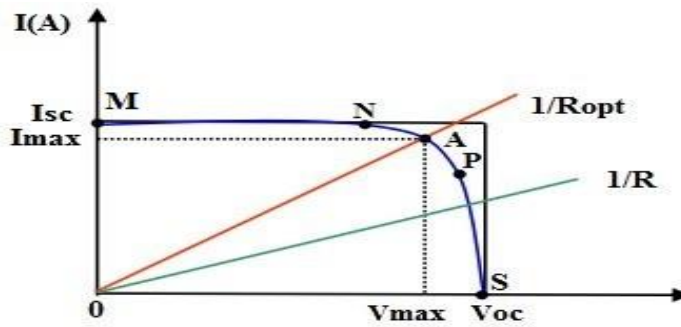


Figure 1.8: A typical current(I-V) curve for a solar cell for different loads.

1.3.2- PV Module

From a practical standpoint, the output power of a single solar cell is insufficient for any useful application in this context, so the overall capability of the PV system should be enhanced by connecting the cells either in series or in parallel. Manufacturers supply PV cells in modules consisting of N_p parallel branches and N_s solar cells in series. The overall objective of this module encapsulation is protecting cells and maximizing the output amount.

Each configuration either series or parallel has its own effect on the output current. Figure 1.9 shows the IV curve of the two configurations.

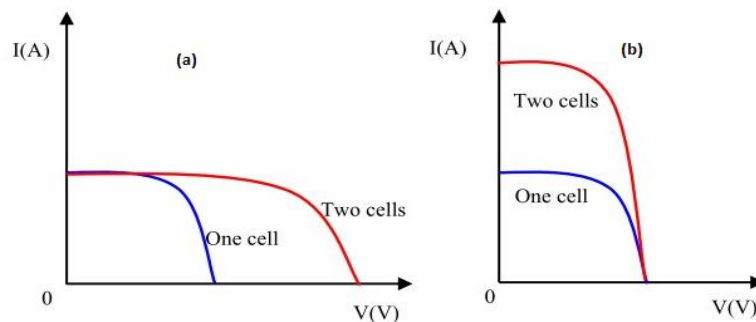


Figure 1.9: Connection of identical PV cells. (a) In series_(b) In parallel.

When connected in series: there is an increase in the overall voltage, when connected in parallel: there is an increase in the overall current. When N_s series

cells are connected, we may calculate the output current of the module using equation (1.8) [8]

$$F(I_{pv}, V_{pv}, T_k, G) = I_{ph} - I_{pv} - I_0 \left[\exp \left(\frac{q(V_{pv} + I_{pv} * R_s)}{N_s * A * K * T_k} \right) - 1 \right] - \frac{(V_{pv} + I_{pv} * R_s * N_s)}{R_p * N_s} = 0 \quad (1.8)$$

1.3.3- PV array

Is the connection of multiple modules in series or in parallel in order to increase the output power of the system either by increasing current or voltage or both at the same time .for modules in series which have the same current , the sum of voltages would be applied to know the entire output voltage , for modules in parallel which have the same voltage the sum of current would be applied to know the entire output current .

When high power is needed the combination of series and parallel modules is required for which the IV total curve would be the sum of individual modules IV curves

The mathematical model of the array can be found using equation (1.9)

$$I = \left(N_{pp} * I_{sc} - N_{pp} * I_0 * \left(e^{\left(\frac{V}{N_s} + \frac{I}{N_{pp}} * R_s \right) * \frac{1}{A * V_T * N_s}} - 1 \right) - \frac{V - \frac{N_{ss} * I * R_s}{N_{pp}}}{R_p} \right) \quad (1.9)$$

Where:

N_{pp} : is the number of modules connected in parallel.

N_{ss} : is the number of modules connected in series.

1.4 Non-Linear characteristics of PV's

The performance of the PV system is highly dependent on the weather conditions mainly the temperature and irradiance which vary momentarily, but affect the characteristics of the array dramatically.

The following figures 1.10, 1.11, 1.12 and 1.13 show the effect of temperature and irradiance on both I-V curve and P-V curve

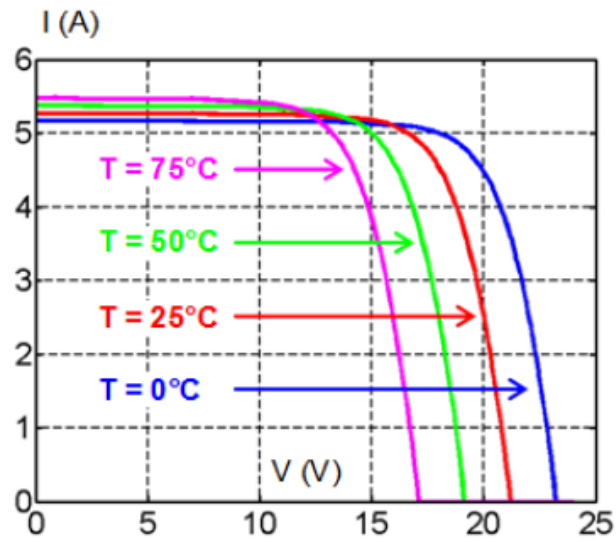


Figure 1.10: Effect of temperature changes on I-V curves.

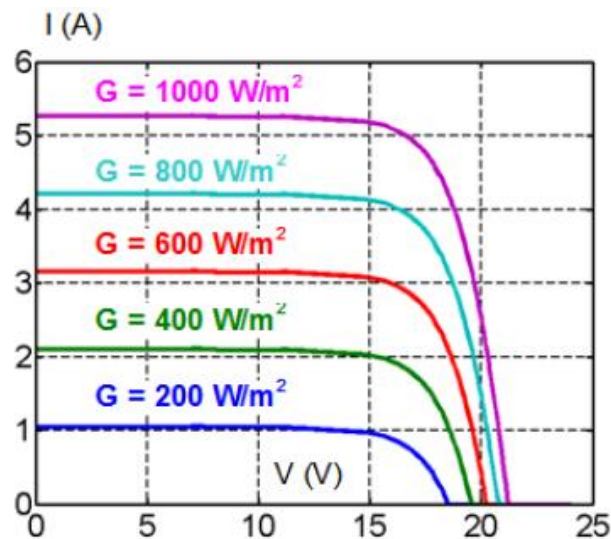


Figure 1.11: Effect of solar irradiance changes on I-V curves.

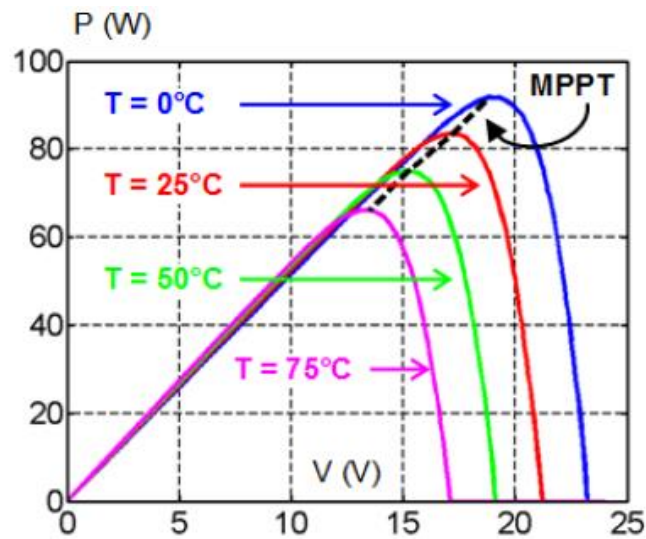


Figure 1.12: Effect of temperature changes on P-V curves.

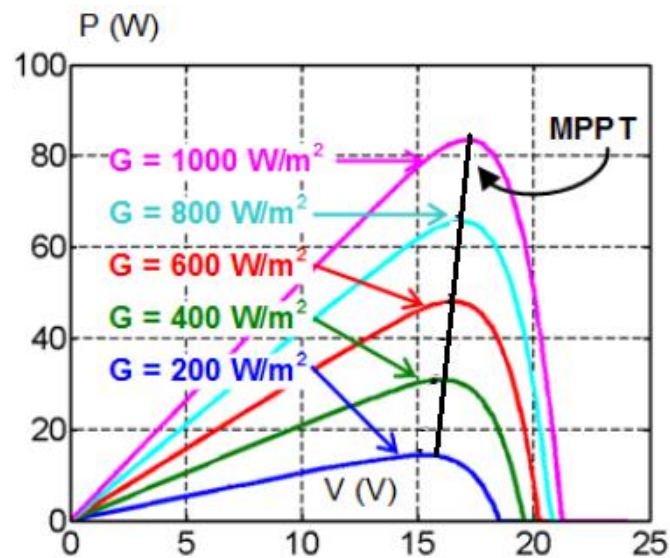


Figure 1.13: Effect of solar irradiance changes on P-V curves.

It is clear from the previous figures that the output power of PV's is directly proportional with the amount of solar irradiance falling on it, and inversely proportional with its temperature. Figures 1.12 and 1.13 show that with the change of the temperature and the solar irradiance the point at which maximum power can be obtained also changes, this means that the array terminal voltage must be varied

using DC-DC converters in order to track the maximum power point. Maximum power point tracking methods will be discussed in details in chapter 2. [9]

1.5 Characteristics of the PV System under Partial Shading

In any outdoor environment, the whole or some parts of the PV system might be shaded by trees, passing clouds, high building, etc., which result in non-uniform insolation conditions. During partial shading, a fraction of the PV cells which receive uniform irradiance still operate at the optimum efficiency. Since current flow through every cell in a series configuration is naturally constant, the shaded cells need to operate with a reverse bias voltage to provide the same current as the remaining cells. However; the resulting reverse power polarity leads to power consumption and a reduction in the maximum output power of the partially-shaded PV module.

Exposing the shaded cells to an excessive reverse bias voltage could also cause “hotspots” to appear in them, and creates an open circuit in the entire PV module. This is often resolved with the inclusion of a bypass diode to a specific number of cells in the series circuit. [10]

figure 1.14 shows the PV under partial shading conditions

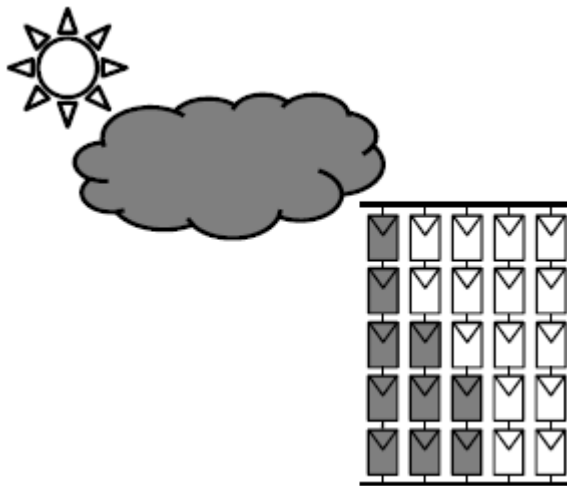


Figure 1.14: PV system under partially shaded conditions caused by passing cloud.

The mathematical model of a module under partial shading can be found by considering $(n-1)$ series cell not shaded and one cell is under partial shading, this cell

has a current $I_{sc} = 0$ hence the voltage across the module can be calculated using equation 1.10

$$V_{SH} = V(n - 1) - (R_p + R_s) I \quad (1.10)$$

Where:

V_{SH} : is the voltage of shaded cell

V_{n-1} : is the voltage of series (n-1) unshaded cells

V_{n-1} can be expressed also as shown in equation 1.11

$$V_{n-1} = \left(\frac{n-1}{n}\right) \cdot V \quad (1.11)$$

Substituting in V_{sh} we obtain equation 1.12

$$V_{sh} = \left(\frac{n-1}{n}\right) V - (R_p + R_s) \cdot I \quad (1.12)$$

Using result of equation 1.12 we can calculate the voltage drop due to partial shading of a cell using equation 1.13

$$\Delta V = V - V_{sh} = V - \left[\left(\frac{n-1}{n}\right) V - (R_p + R_s) \cdot I \right]$$

$$V_{n-1} \Rightarrow \Delta V = \frac{V}{n} + (R_p + R_s) I \quad (1.13)$$

Taking $R_p \gg R_s$ We can find

$$\Rightarrow \Delta V = \frac{V}{n} + R_p \cdot I$$

The power drop due to partial shading on one cell can be found using equation 1.14

$$P = \Delta V \cdot I \quad (1.14)$$

- **The Bypass diode and Blocking diode:**

the problem of partial shading is often resolved with the inclusion of a bypass diode to a specific number of cells in the series circuit. Figure 1.15 shows the connection of bypass diodes into an array of 3 parallel strings holding 4 series modules each.

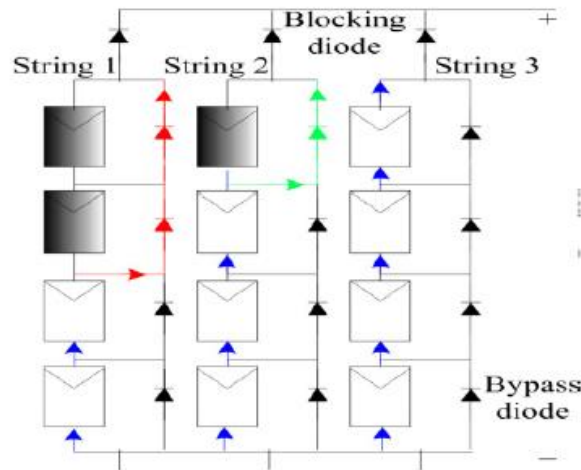


Figure 1.15: the connection of bypass and blocking diodes to a PV array.

Figure 1.16 shows the Power-voltage curve of each string with: string 1 under partial shading of 2 modules, string 2 partial shading of 1 module and last string 3 without shading.[12]

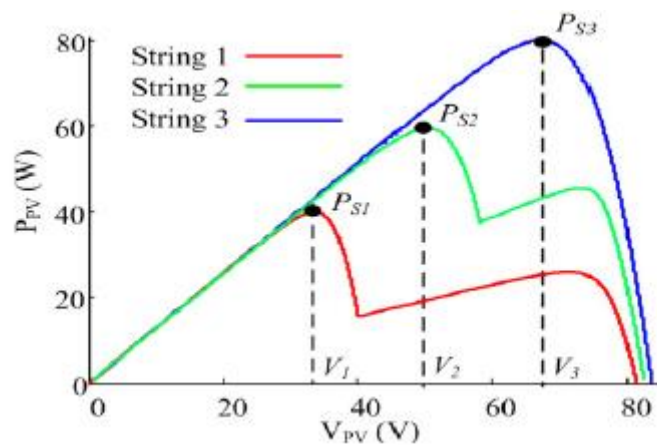


Figure 1.16: Power-voltage curve of each string under partial shading.

It is important to note that the characteristics of an array with bypass diodes differ from the one without these diodes. Since the bypass diodes provide an

alternate current path, cells of a module no longer carry the same current when they are partially shaded. Therefore, the power-voltage curve develops multiple maxima.

Unfortunately presenting multiple maxima in the P-V characteristic is a crucial issue and most of the conventional MPPT algorithms may not distinguish between the local and global maxima.

Figure 1.17 shows how the extractable maximum power point differs in PV array with and without bypass diodes.[11]

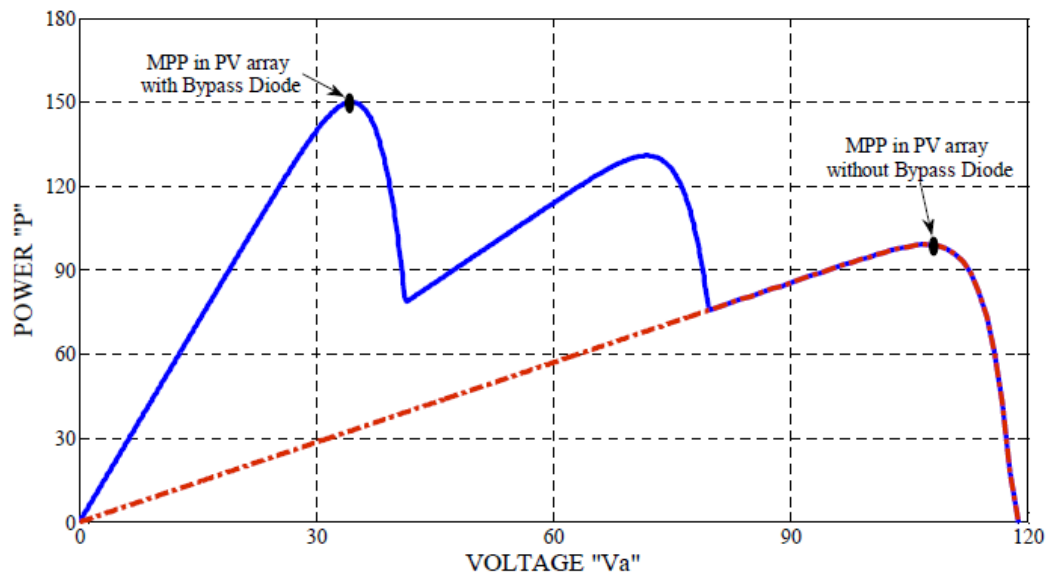


Figure 1.17: Power-voltage curve of a PV array under partial shading with and without bypass diode.

- **The Blocking diode:**

In a solar power system consisting of more than one string connected in parallel, if a short circuit occurs in one of the strings, the blocking diode prevents the other PV strings to discharge through the short-circuited string.

1.6 Conclusion

In this chapter we have introduced the photovoltaic principles and models and observed the effect of the environment on this technology and the solutions that have been used until now to overcome these drawbacks, where the bypass diode have been used in partial shading conditions. However due to its drastic effect on the PV characteristics, the tracking of the maximum power point of the curve became imminent. Many researches were conducted in this field and multiple algorithm were tested in order to develop the most efficient MPPT controller to increase the efficiency of the system.

Chapter Two

Maximum power point tracking MPPT

2.1 Introduction

One of the most important optimizations in a solar system is the maximum power point tracking (MPPT). In a photovoltaic system it aims to maximize the power delivered from the panels to the load. Power output from the PV panel is constantly varying with different temperatures and irradiances. At a given temperature and irradiance the PV panel has a unique maximum power output value called the maximum power point (MPP). Tracking it is essential for instance on winter days where sunlight is available for just few hours ,therefore it becomes necessary to maximize the power output from the panels to be able to charge batteries as fast as possible.

In this chapter we will introduce the critical elements that form an MPPT system : the DC/DC converter, the feedback system, the PV power source, the load ,and the control unit into which three algorithms are considered: a conventional algorithm, the Incremental Conductance and two new algorithms which are Golden Section Search GSS and the PSO (particle swarm optimisation).

2.2 Maximum power point tracking

The maximum power output from the PV is highly varying with temperature and irradiance, with such constantly changing variables no fixed values can be assigned in advance for the maximum power points.

MPPT algorithms which run on a controller tracks this MPP through different techniques by sensing the input and producing an output that operates the system at the critical point or a value close to it. All MPPT algorithms operate on automatically finding V_{mpp} and I_{mpp} that correspond to the Maximum power point.

Figure 2.1 consists of a PV panel from which the voltage and current values are sampled, a controller that runs the MPPT algorithm to adjust the voltage, a pulse width modulation unit that sends the appropriate signal to the DC/DC converter changing the voltage thus changing the output power. Finally, the power is supplied to a battery or Inverter to be inverted to AC form.

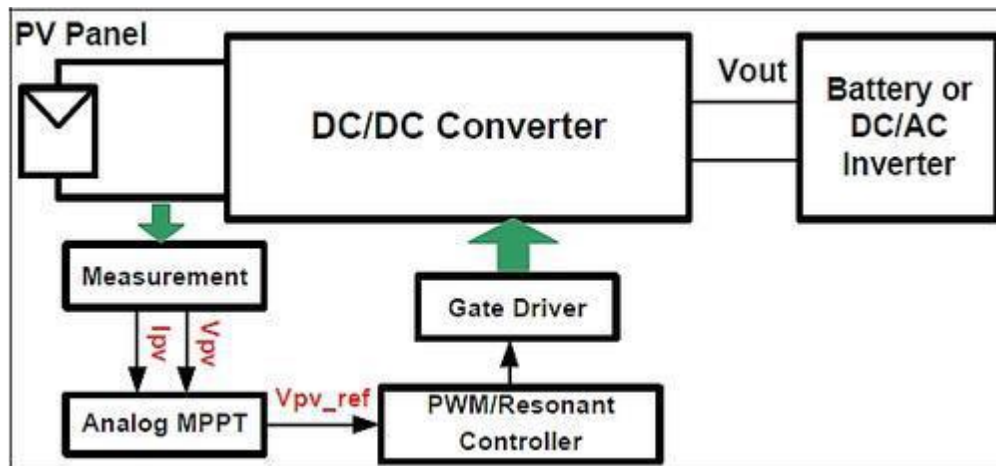


Figure 2.1: MPPT tracking system.

2.3 MPPT Components

2.3.1- Controller

The part of the PV system that tracks the MPP is the controller which implements an algorithm that keeps track of the maximum power point by sensing the inputs and sending the appropriate control signal to the chopper to adjust the voltage that corresponds to the V_{mpp} the voltage value of the maximum power point to operate at R-optimum the equivalent resistance value of the maximum power point.

2.3.2- DC/DC Converter

When proposing an MPP tracker the major job is to choose and design a highly efficient converter which is supposed to operate as the main part of the MPPT, among the topologies available the buck boost converter is the only one which allows the follow-up of the PV module maximum power point regardless of temperature, irradiance and connected load. It provides the opportunity to have either higher or lower output voltage compared with the input voltage, it is cheap, and widely used in MPPT systems.

The proposed DC-DC buck boost converter with minimal number of switches is shown in figure 2.2

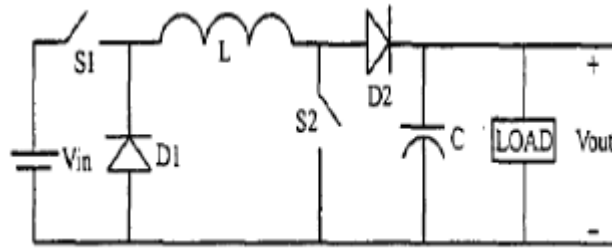


Figure 2.2: Proposed DC-DC buck-boost converter.

The control of the output from the DC-DC converter is based on the input signal to the electronic switch this input signal is called the duty cycle.

The Duty cycle defined by the ratio between the electronic switch is ON (closed) and the total switching period. Thus, the duty cycle value lies in the following range

$$0 < \text{Duty cycle} < 1$$

The total period of switching is shown in equation 1

$$T = t_{on} + t_{off}$$

The Duty cycle can be computed using equation 2

$$d = t_{on} / T$$

figure 2.3 shows the computation of the duty cycle using pulses

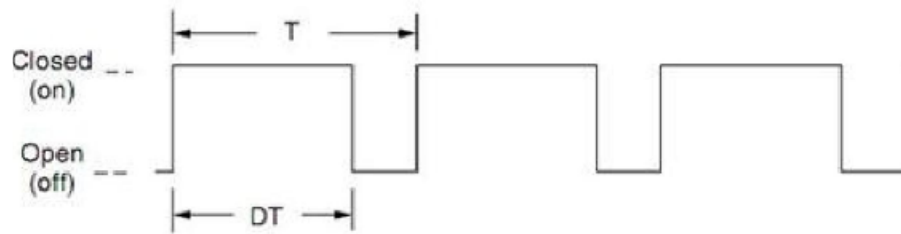


Figure 2.3: Sample switching pulse.

2.3.3- Pulse Width Modulation Unit (PWM)

It is the unit that actually feeds the input duty cycle to the converter switch. The main advantage of PWM is that power loss in the switching devices is very low. When a switch is off there is practically no current, and when it is on, there is almost no voltage drop across the switch. Power loss, being the product of voltage and current, is thus in both cases close to zero. PWM also works well with digital controls, which, because of their on/off nature, can easily set the needed duty cycle.

2.4 MPPT Algorithms

Various algorithms have been implemented to track the MPP, each algorithm has its own advantages and drawbacks. Algorithms can vary in their complexity, area used, power consumption, convergence, speed, and other aspects. The algorithms have been classified as conventional such as P&O or incremental conductance that hardly differentiate between local and global maxima or as new MPPT techniques such as Golden Section Search Algorithm (GSS), Particle Swarm optimization (PSO).

2.4.1- Incremental Conductance

This method uses the PV array's incremental conductance $\frac{dI}{dV}$ to compute the sign of $\frac{dP}{dV}$. When $\frac{dI}{dV}$ is equal and opposite to the value of I/V (where $\frac{dP}{dV} = 0$) the algorithm knows that the maximum power point is reached and thus it terminates and returns the corresponding value of operating voltage for MPP. This method tracks rapidly changing irradiation conditions more accurately than P&O method. One complexity in this method is that it requires many sensors to operate and hence is economically less effective [14] and [15].

$$P=V*I \quad (2.1)$$

Differentiating w.r.t voltage yields:

$$\frac{dP}{dV} = \frac{d(V*I)}{dV} \quad (2.2)$$

$$\frac{dP}{dV} = I * \left(\frac{dV}{dV}\right) + V * \left(\frac{dI}{dV}\right) \quad (2.3)$$

$$\frac{dP}{dV} = I + V * \left(\frac{dI}{dV}\right) \quad (2.4)$$

When the maximum power point is reached the condition would be:

$$\frac{dP}{dV} = 0 \quad (2.5)$$

$$I + V * \left(\frac{dI}{dV}\right) = 0 \quad (2.6)$$

$$\frac{dI}{dV} = \frac{-I}{V} \quad (2.7)$$

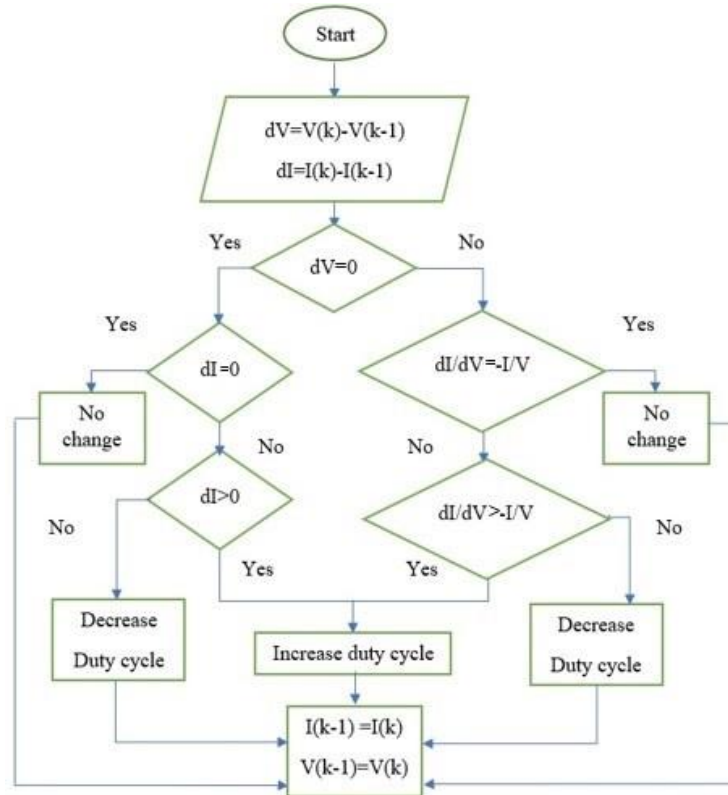



Figure 2.4: Flowchart of the IC method with direct control.

In figure 2.4, $V(k)$ is the new measured voltage and $I(k)$ is the new measured current, $V(k-1)$ and $I(k-1)$ are the previous measured values. When the new value is injected into the program, the previous value and the new one is compared, then it determines if the voltage differential is zero or not. According the voltage differentials if it is zero, the current difference can be determined if it is zero or not. If both of them are zero, it means that they have the same value of impedance and the value of duty ratio will remain the same as before. If the voltage differential is zero, but the current differential is not zero, it means that the insolation has changed. When the difference of the current values is greater than zero, the duty cycle will be increased, when the difference of the current value is less than zero the duty cycle will be decrease, If the voltage differential is not zero we check whether it satisfy the equation 2.7 or not, when equation 2.7 is satisfied the slope of the power curve will be zero, that means the system is operating at MPP, if the variance of conductance is greater than the negative conductance values, it means the slope of the power curve is positive and the duty cycle is to be increased, otherwise it should be decreased [16], [17].

2.4.2- Golden Section Search GSS:

Golden Section Search method is an optimization technique. This technique is based on shrinking sequentially the interval inside which the optimum is located. Two points X_1 , X_2 , are selected within the interval such that each point subdivides the interval into two parts satisfying: [21],[22].

Length of the line / Length of larger fraction = Length of larger fraction / Length of smaller fraction



$$\frac{L}{L_1} = \frac{L_1}{L_2} \quad (L = L_1 + L_2) \quad (2.8)$$

taking $\frac{L_2}{L_1} = R$

the equation will be $1 + R = \frac{1}{R}$ or $R^2 + R - 1 = 0$

The solution of this equation is: $R=0.618$ which is the golden ratio. The previous result leads to the following equations 2.9 and 2.10 of X_1 and X_2 :

$$X_1 = a + 0.618(b-a) \quad (2.9)$$

$$X_2 = b - 0.618(b-a) \quad (2.10)$$

The function $f(x)$ in interest is evaluated at these points X_1, X_2 .

➤ If $f(X_1) < f(X_2)$, the abscissa of the maximum point cannot be less than X_1 . Thus, we may conclude that the maximum is in the range of $(X_1, b]$ which is taken as the new interval for the next iteration.

➤ Else, if $f(X_1) > f(X_2)$, the maximum's abscissa must be less than X_2 . Therefore, the maximum must lie in the range $[a, X_2)$, the interval taken in the next iteration. The process is continuously repeated until the difference $|X_1 - X_2|$ is less than a certain chosen precision, the resultant maximum's abscissa is given at point

$$X_0 = \frac{1}{2} (X_1 + X_2). \quad (2.11)$$

Figure 2.5 shows the flowchart of the implemented algorithm

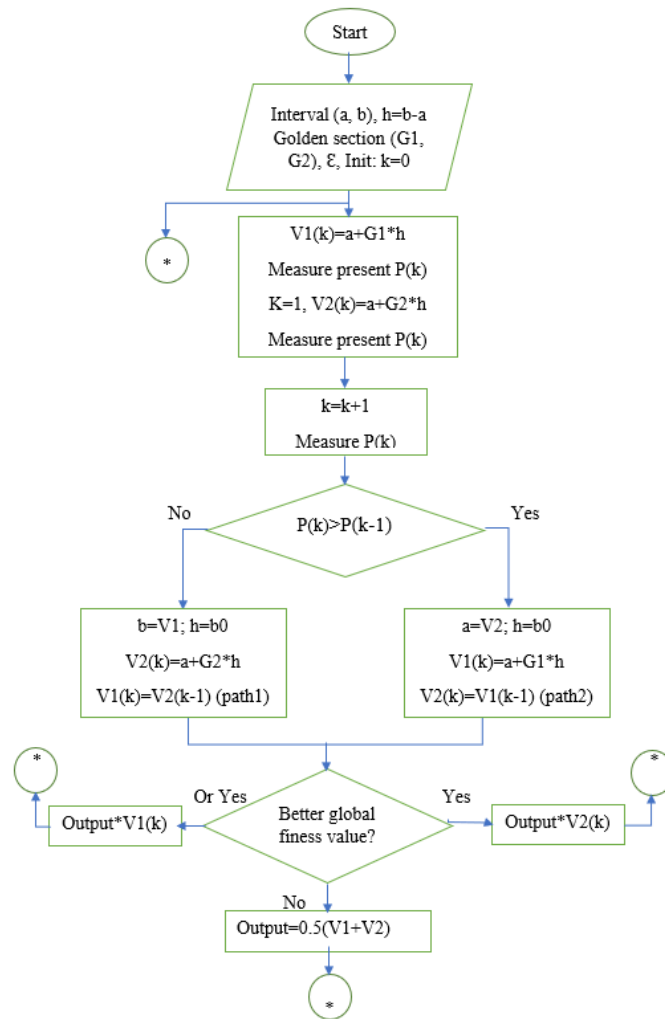


Figure 2.5: Flowchart of the GSS method.

2.4.3- Particle Swarm Optimisation PSO:

PSO is simple robust, intelligence optimization and meta heuristic approach, proposed in 1995, it is a type of Evolutionary Algorithm (EA) search optimization technique; originated by the attitude of the birds in group to solve the difficulties involved in optimization or search process.[18]

PSO uses a number of agents (particles) that constitute a swarm moving around in the search space looking for the best solution; each particle keeps track of its coordinates in the solution space which are associated with the best solution (fitness

function) that has been achieved so far by that particle. This value is called personal best: Pbest, another best value that is tracked by the PSO is the best value obtained so far by any particle in the neighbourhood of that particle; this value is called Gbest.

During the optimization process, the particles take up the objective function's values, while their Gbest and Pbesti are saved. The basic PSO algorithm which determines the next velocity and position of the candidate solution can be given mathematically by equations (2.11) and (2.12)

$$V_i^{k+1} = w * V_i^k + r_1 * c_1 * (P_{besti} - x_i^k) + r_2 * c_2 * (G_{best} - x_i^k) \quad (2.11)$$

$$x_i^{k+1} = x_i^k + V_i^{k+1} \quad (2.12)$$

Where:

i: represents the variable of the optimization vector,

k is the number of iterations

V_i^k and x_i^k : the velocity and position of the ith variable within k iterations

W: is known as inertia that maintains a

balance between the local and global search.

c 1 and c 2: are acceleration constants.

r 1 and r 2: are two generated random numbers uniformly distributed in the interval [0-1].

The variable Pbesti records the best position affected by the ith particle up to the exact time of measurement. The equation (2.13) indicates that this position is only recorded as Pbesti if the condition stated below is satisfied.

$$P_{besti} = x_i^k \text{ if } \text{fit}(x_i^k) \geq \text{fit}(p_i) \quad (2.13)$$

Figure 2.6 shows how the vectors are related to obtain the new velocity and displacement during an optimisation process

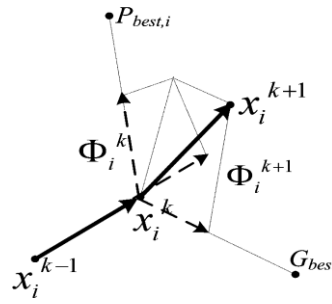


Figure 2.6: Movement of particles in the optimization process.[20]

The steps that are involved in PSO algorithm for extracting GMPP are as follow:

- ❖ Initially, PSO originates random particles in a search space. Where the velocity of each particle is also randomly chosen.
- ❖ PSO evaluates the fitness function for each particle using equation (2.11).
- ❖ PSO Finds out the particles personal and best global solution amongst entire particles.
- ❖ It Evaluates and informs the velocity and position of each particle for current iteration.
- ❖ If the condition of convergence is fulfilled, PSO stops the search process, if the condition is not fulfilling then it rises the iteration count and once again starts the evolution of fitness process.[19]

❖ PSO in maximum power tracking principle:

In this project the PSO has been used in the research of the maximum power point and the Generation of the duty cycle depending on the MPPT, this algorithm has been implemented following the steps:

- 1- Generating the swarm: by defining the initial particle position as the duty cycle and the initial particle velocity as the incrementation in the duty cycle i.e Δd .
- 2- Initializing the values of the constants of PSO & the initial powers are usually taken randomly for the proposed algorithm the particles are initialised at fixed and equidistant points within the predefined interval $[0-V_{oc}]$
- 3- Evaluating the fitness function: the function is evaluated after each time the particle is injected i.e. the duty cycle, the power can be computed from the voltage and current corresponding to the duty cycle

- 4- Determining of Pbest and Gbest: each particle has its own Pbest and each swarm has Gbest which would be the best of all particles in the swarm.
the new Pbest and Gbest are compared with the previous swarm's Pbest and Gbest
- 5- Updating the velocity and the position of each particle using equations (2.8) and (2.9)
- 6- Checking the convergence: if the final criterion is met the algorithm converges and stops the computation, otherwise, a new iteration is performed keeping in memory the results obtained from the previous iteration, steps from 2 up to 6 are performed.

Figure 2.7 shows the flowchart of the implemented algorithm

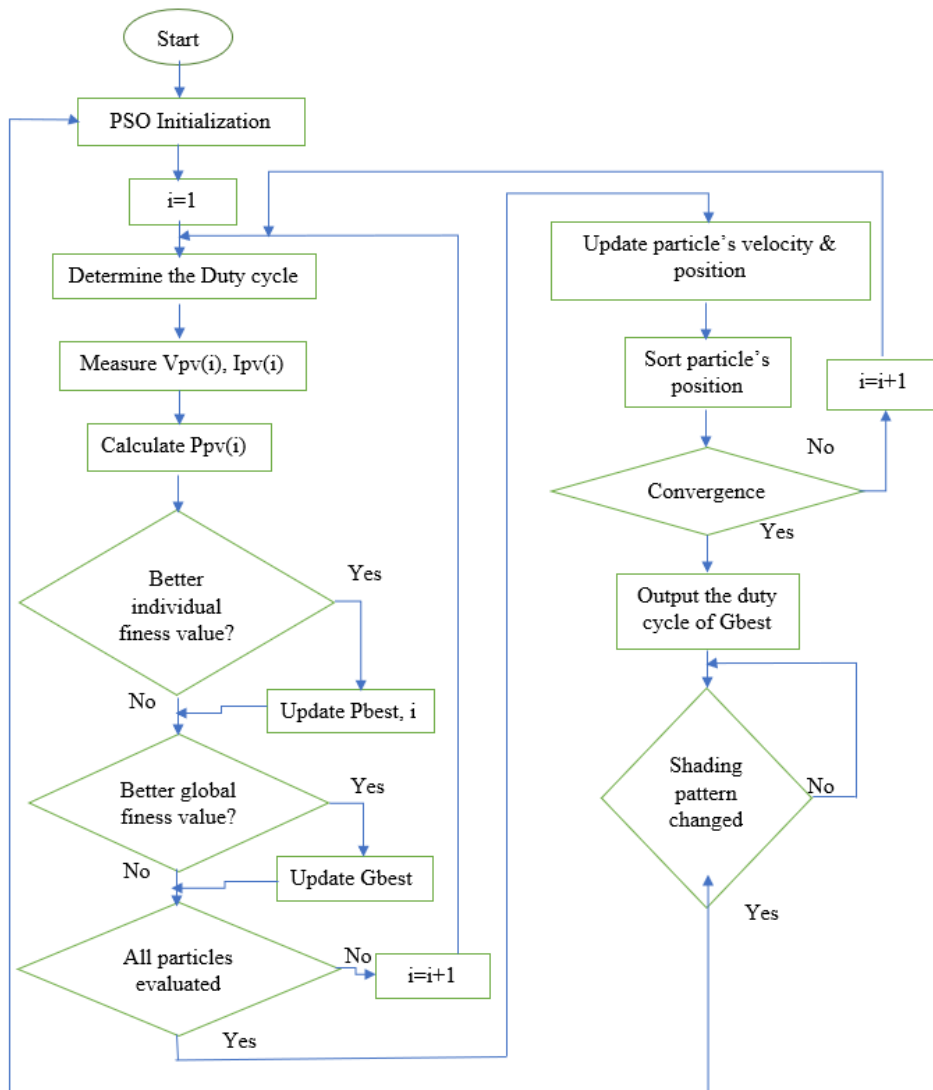


Figure 2.7: Flowchart of PSO based on GMPPT.[20].

2.5 Conclusion

In this chapter we have seen three algorithms which are widely used in MPPT, a conventional one which is the incremental conductance and two algorithms, the Golden section algorithm and the PSO. These three algorithms are to be tested in the next chapter to compare their efficiencies under normal and partial shading conditions.

Chapter Three

Simulation and Results

Figure 3.1: Simulink model of a single PV module.

Figure 3.2 shows the obtained curves from the simulation of the previous model

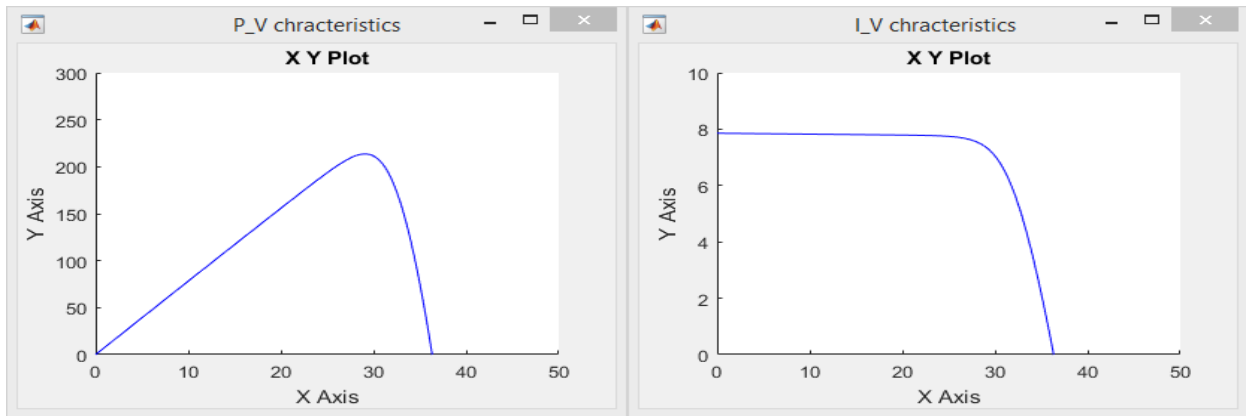


Figure 3.2: P-V and I-V characteristics of a single module.

Figure 3.3 shows the simulation results of an array of 5 similar modules in series.

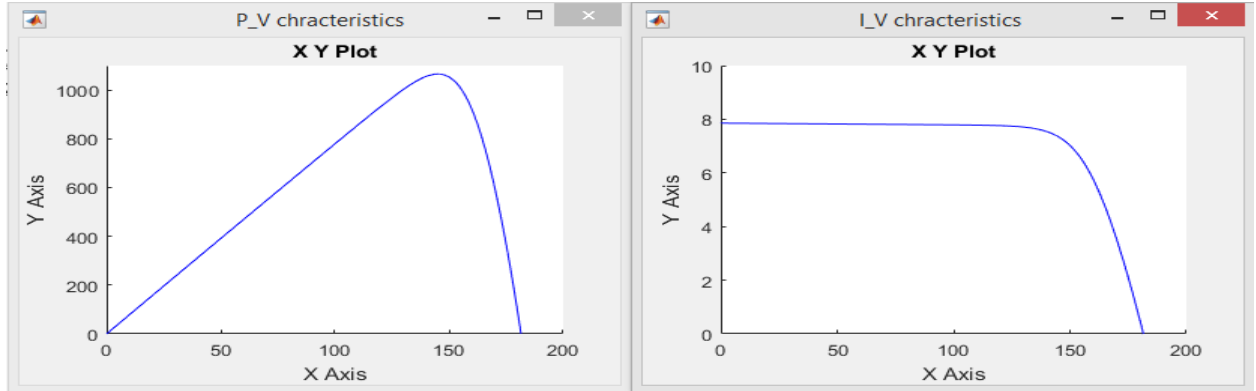


Figure 3.3: P-V and I-V characteristics of 5 modules in series.

We notice that the maximum power point of five modules under uniform irradiance is five times the one of a single module that is 213.15V.

3.2.2- PV module characteristics under partial shading condition:

Under partial shading using bypass diodes the model exhibits multi peaks characteristics due to the diode effect on the current and hence on the power.

Figures 3.4 and 3.5 show the Simulink model of 5 modules in series under partial shading connected to bypass diodes, and their I-V and P-V characteristics in these conditions

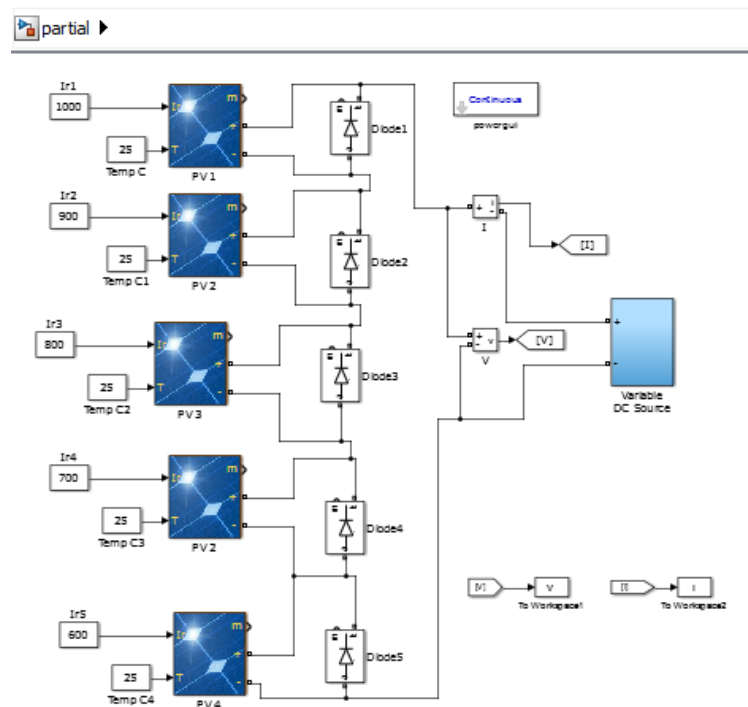


Figure 3.4: Simulink model of 5 modules in series under PS with bypass diodes.

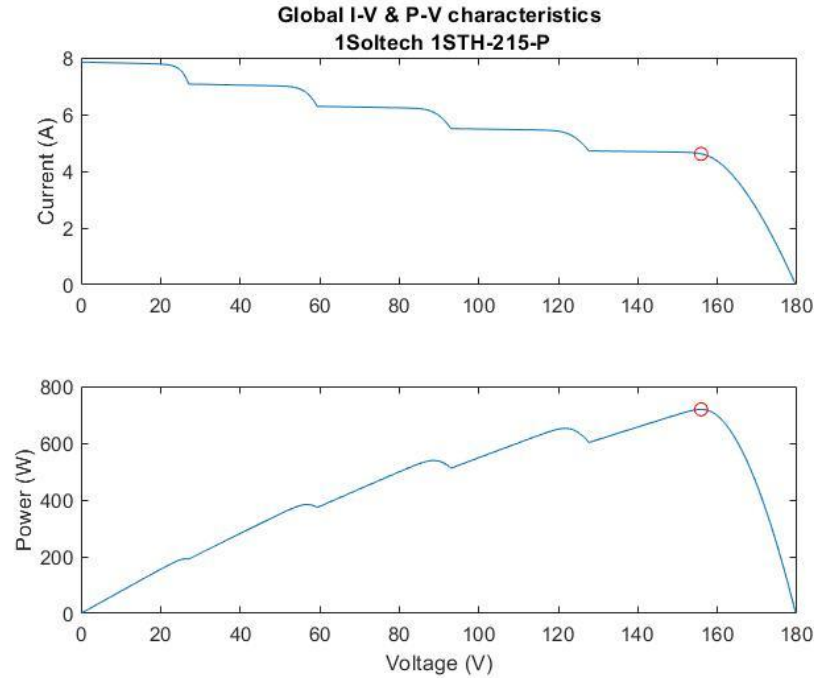


Figure 3.5: I_V and P_V curves of 5 modules in series under PS with bypass diodes.

Due to non-uniform solar irradiance we notice that the P-V & I-V curves exhibit multi-peaks.

3.3 Presentation of the system with MPPT Controller

3.3.1 Non inverting buck-boost converter (DC-DC converter):

To simulate a non-inverting DC-DC converter we have chosen to work with the electrical elements that are available in the market to ensure better results that can be confirmed with the implementation.

We have modeled the buck boost converter using a constant dc voltage source and a duty cycle comparator. The parameters of Dc source, the capacitor, the inductor and the switch are listed below:

- Inductance $H = 250 \text{ e-6 (H)}$
- Ideal switch:
 - Internal resistance R_{on} (Ohms): 0.001
 - Initial state (0 for 'open' 1 for closed): 0
 - Snubber resistance R_s (Ohms): $1\text{e}5$
 - Snubber capacitance C_s (F): inf
- Capacitor $C = 1000 \text{ e-3 (F)}$
- Source: $V_{dc} = 213.15 \text{ V}$ (the V_{mp} of our PV module)

Figure 3.6 shows the model of the non-inverting DC-DC chopper with its control

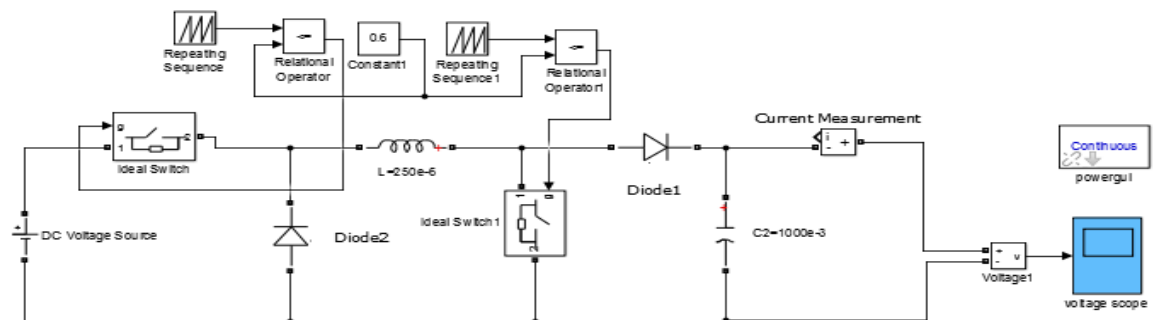


Figure 3.6: Simulink model of a non-inverting buck boost converter.

Figure 3.7 shows the obtained voltages from the dc chopper where the voltage has been boosted from 213.15 to approximately 410V. and Then bucked from 213.15 to approximately 105 V.

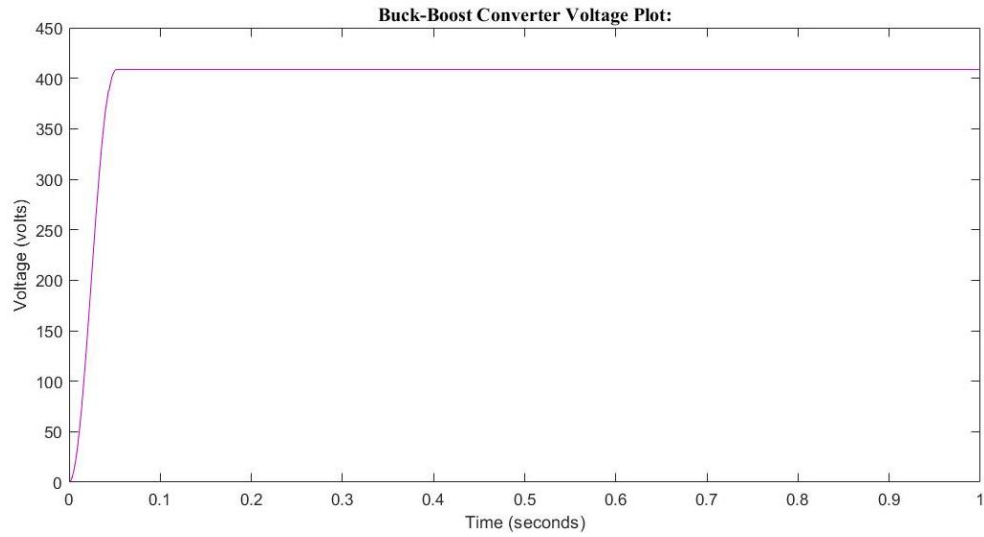


Figure 3.7.a: Output voltage of a non-inverting buck-boost converter.

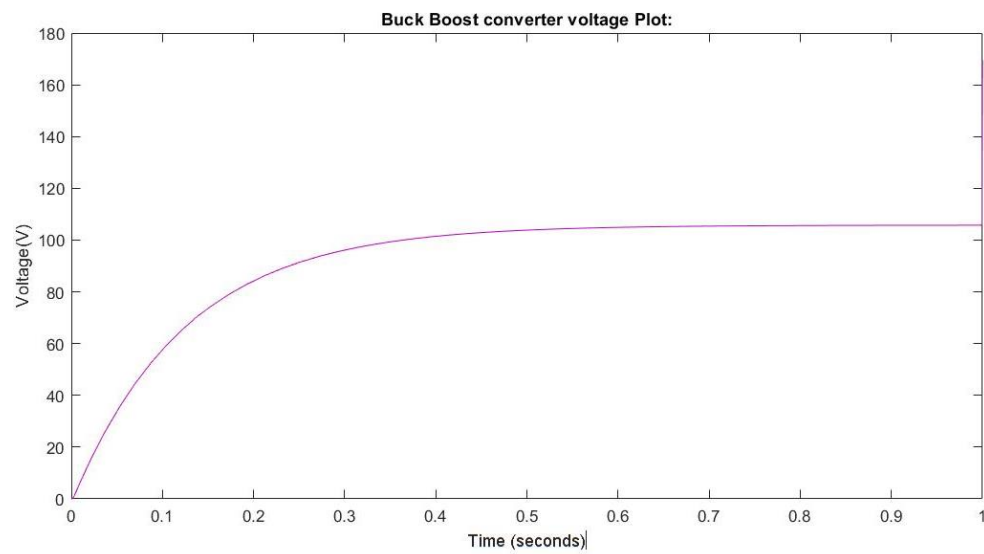


Figure 3.7.b: Output voltage of a non-inverting buck-boost converter.

3.3.2 Incremental Conductance

3.3.2.1- Incremental Conductance MPPT for a Single Module-under uniform conditions:

To test the incremental conductance tracking method, we have integrated a MATLAB code as a function, which accepts the V_{pv} and I_{pv} as inputs from the system and generates a reference voltage (V_{ref}) that is to be compared with V_{pv} to generate the duty cycle which controls the DC –DC converter switches.

First, we have defined the initial values as shown in table 3.2

| V(initial) | V(max) | V(min) | Delta V |
|------------|--------|--------|---------|
| 5 | 50 | 5 | 0.5 |

Table 3.2: Initialization of parameters for a single module.

Under Uniform conditions we have used a customized profile of irradiance as shown in table 3.3

| | | | |
|--------------------------------|------|-----|-----|
| Irradiance (w/m ²) | 1000 | 600 | 800 |
|--------------------------------|------|-----|-----|

Table 3.3: Irradiance profile under uniform conditions.

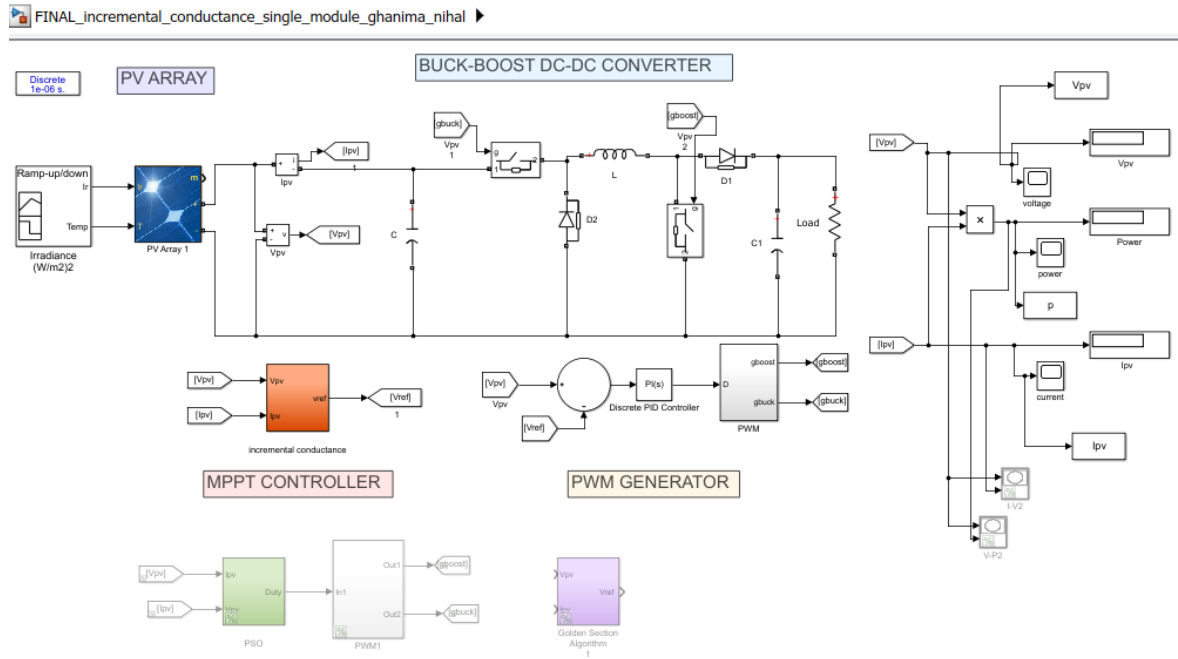


Figure 3.8: Simulink model of a PV module using MPPT controllers.

Figures 3.9 3.10 & 3.11 shows the voltage, current & power curves of simulation results

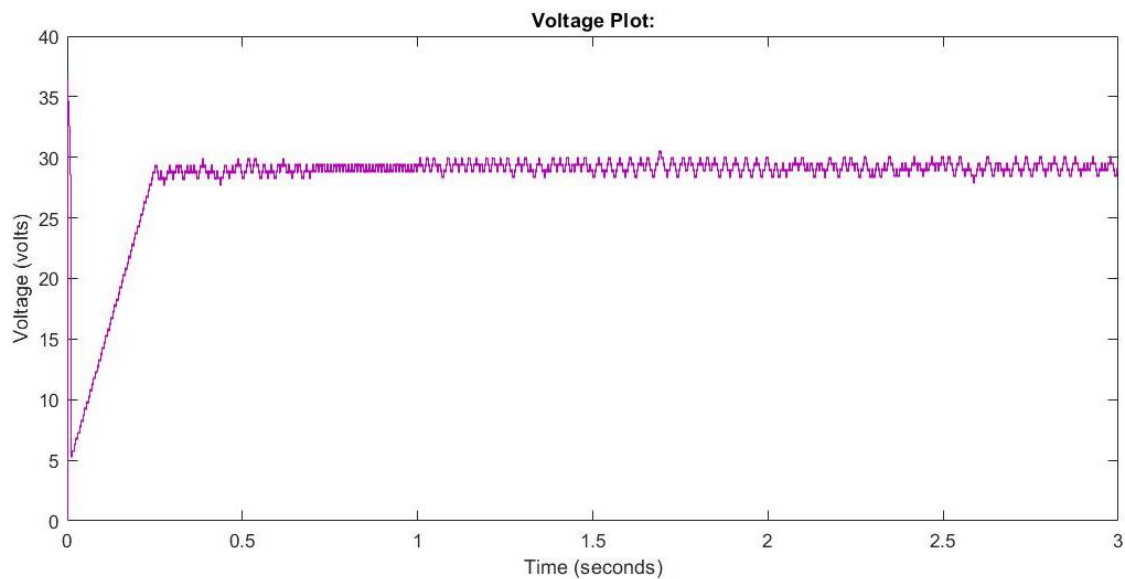


Figure 3.9: Voltage curve of single PV module using incremental conductance MPPT.

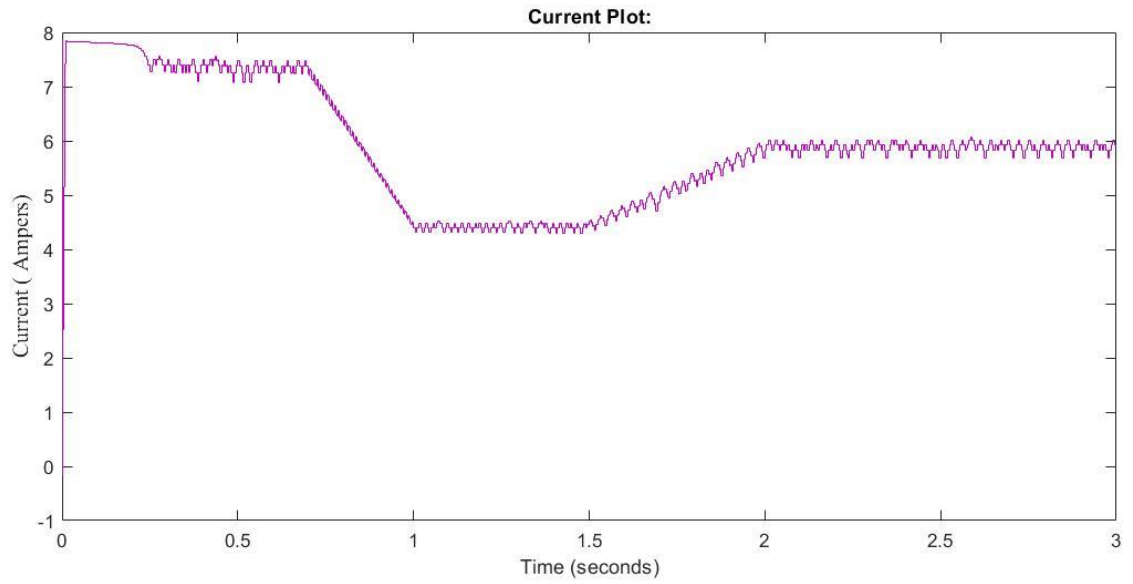


Figure 3.10: Current curve of single PV module using incremental conductance MPPT.

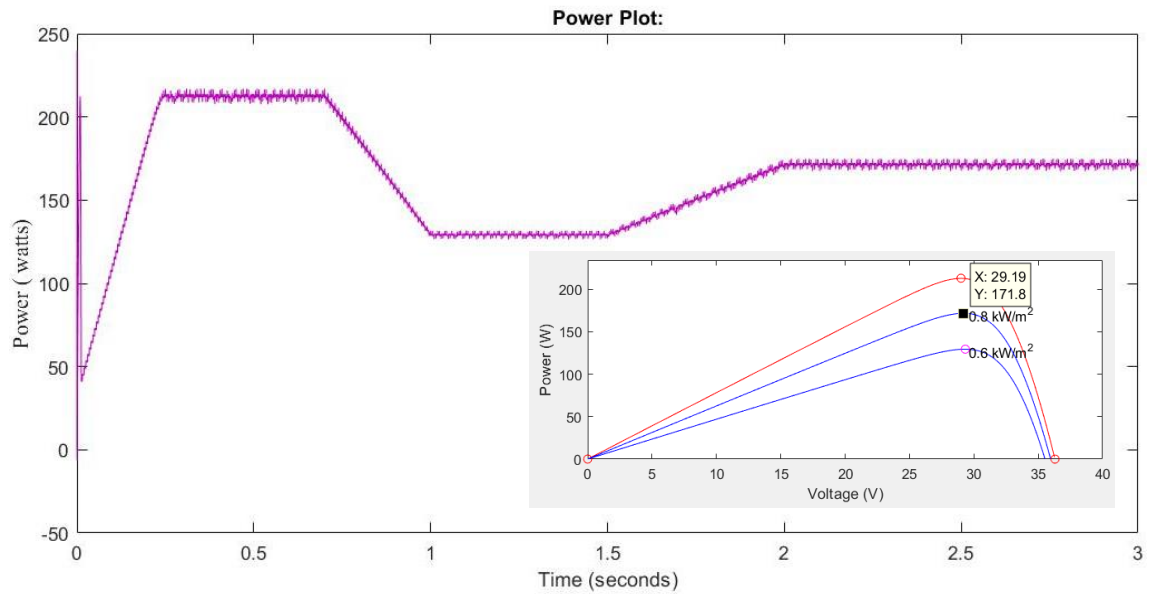


Figure 3.11: Power curve of single PV module using incremental conductance MPPT.

3.3.2.2- Incremental Conductance MPPT for Five Series Modules- under uniform conditions:

To verify the efficiency of our system we have used several modules in series joined with bypass diodes to obtain daily life conditions (with partial shading).

Two experiments were performed using the incremental conductance controller, the first simulation is at uniform conditions for the 5 series modules i.e. the same temperature & irradiance variation for all the modules, the second simulation is under partial shading i.e. The 5 series modules are at non-uniform irradiance.

for 5 series modules with bypass diodes the initializations used in incremental algorithm is shown in table 3.4

| V(initial) | V(max) | V(min) | Delta V |
|------------|--------|--------|---------|
| 70 | 152 | 15 | 0.5 |

Table 3.4: Initialization parameters for 5 series modules.

Figure 3.12 shows the overall system of 5 series connected modules with bypass diodes using incremental conductance controller

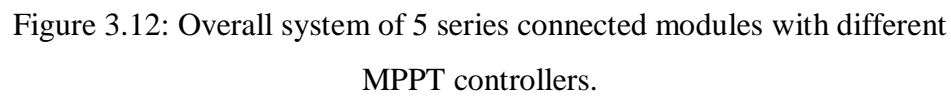


Figure 3.13: Voltage curve of five PV modules under uniform conditions using incremental conductance MPPT.

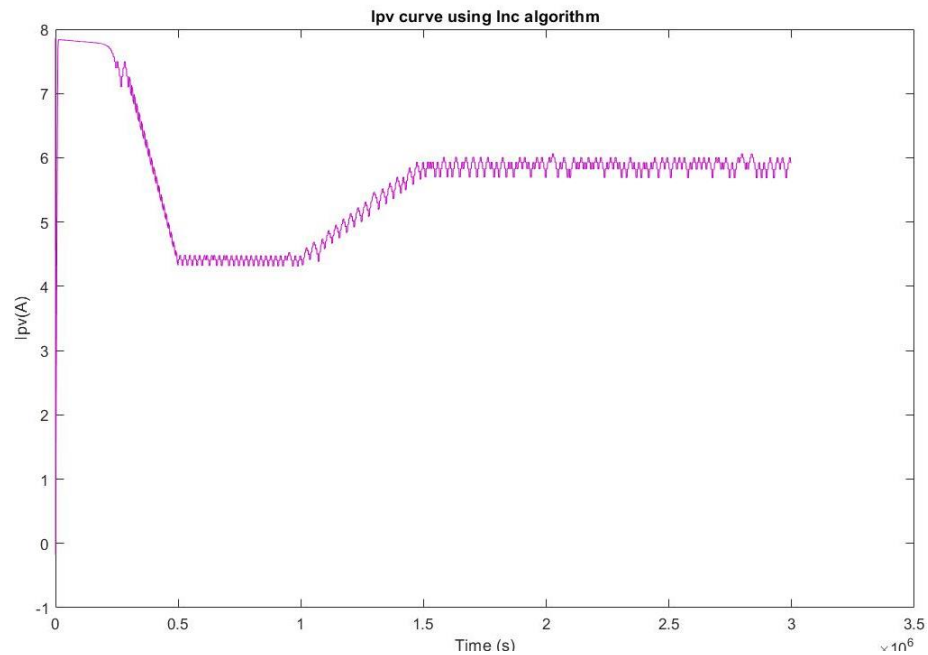


Figure 3.14: Current curve of five PV modules under uniform conditions using incremental conductance MPPT.

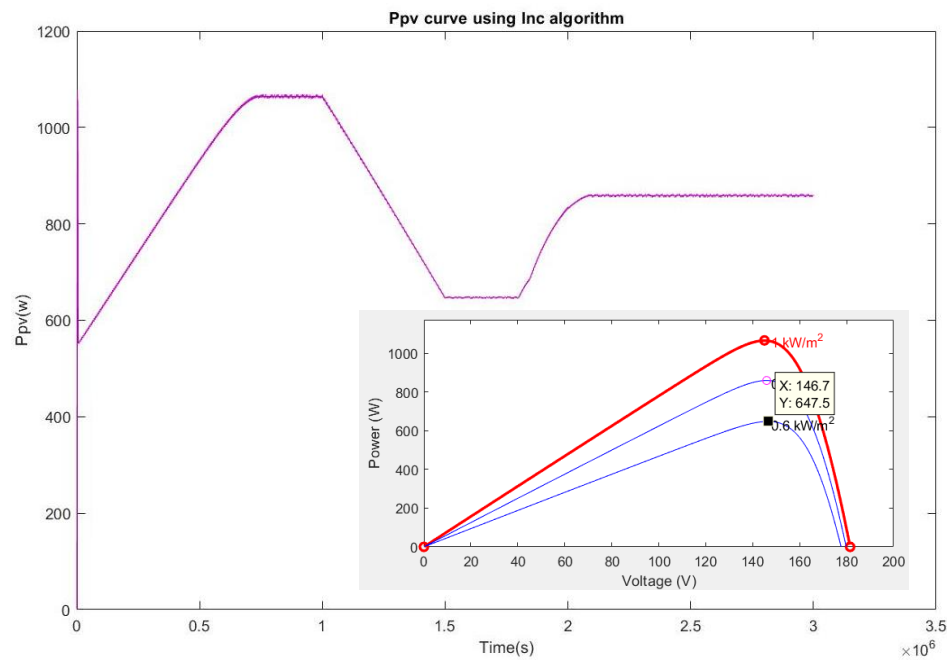


Figure 3.15: Power curve of five PV modules under uniform conditions using incremental conductance MPPT.

3.3.2.3- Incremental Conductance MPPT for Five Series

Modules- under Shading conditions:

Figures 3.16 3.17 & 3.18 show the voltage current & power curves of 5 modules under partial shading using INC Controller

Under non-uniform conditions we have used a customized profile of irradiance as shown in table 3.5

| Irradiance(w/m ²) | 1000 | 900 | 800 | 700 | 600 |
|-------------------------------|------|-----|-----|-----|-----|
|-------------------------------|------|-----|-----|-----|-----|

Table 3.5: Irradiance profile under non-uniform conditions for 5 series modules.

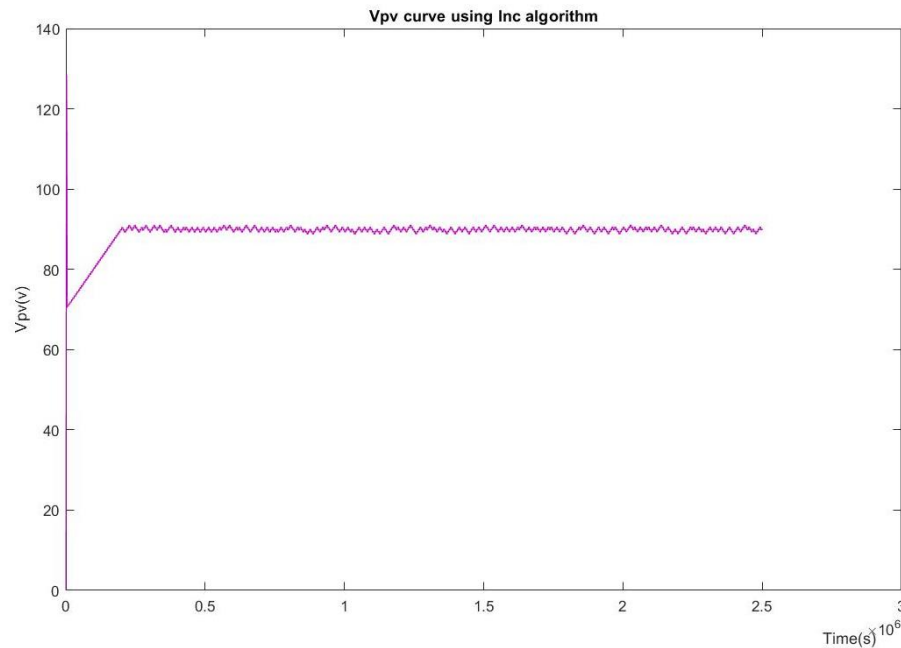


Figure 3.16: Voltage curve of five PV modules under non-uniform conditions using incremental conductance MPPT.

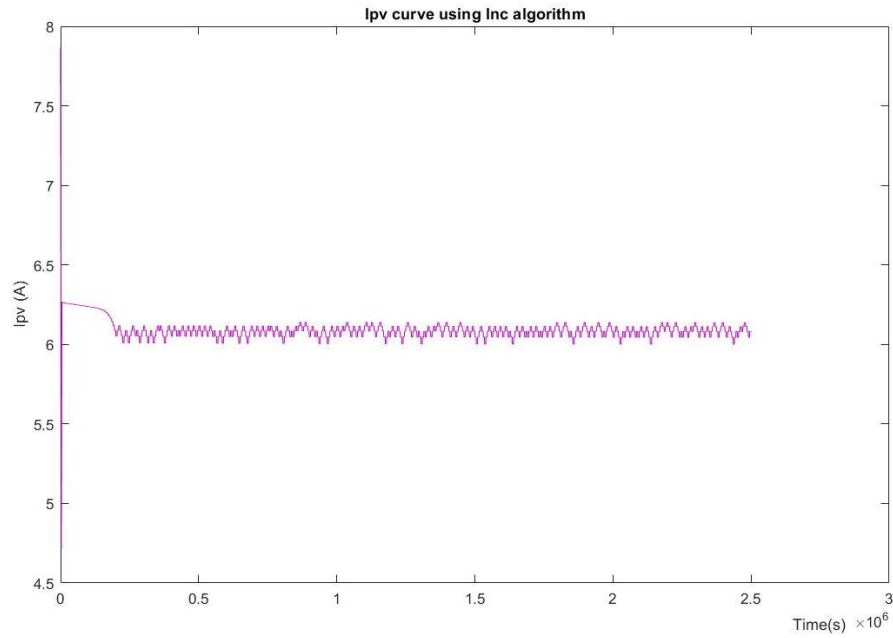


Figure 3.17: Current curve of five PV modules under non-uniform conditions using incremental conductance MPPT.

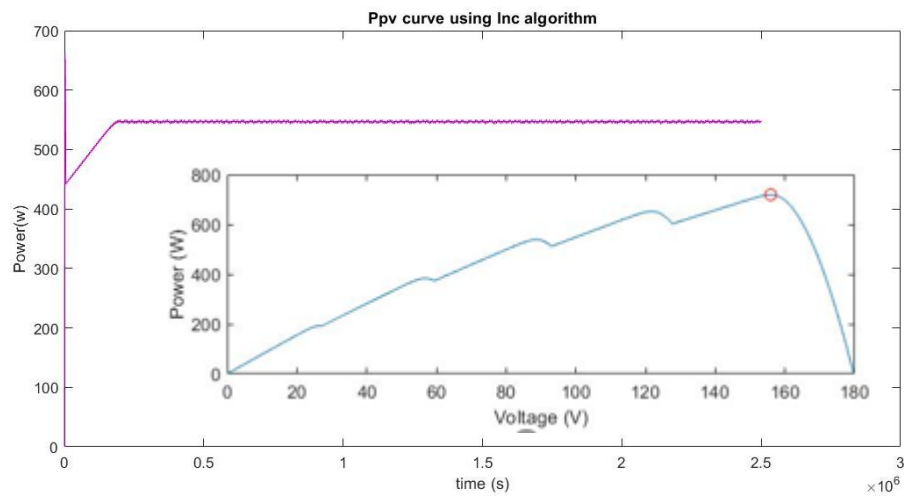


Figure 3.18: Power curve of five PV modules under non-uniform conditions using incremental conductance MPPT.

3.3.3 Golden Section Search GSS

3.3.3.1- GSS MPPT for a Single Module- under uniform conditions:

The second algorithm to be used is the golden section search instead of incremental conductance with approximately same approach and same profile of irradiance of table 3.3 as well as the initial values as shown in table 3.2.

Figures 3.19 3.20 & 3.21 show the voltage, current & power curves of a single module under uniform irradiance using GSS Controller

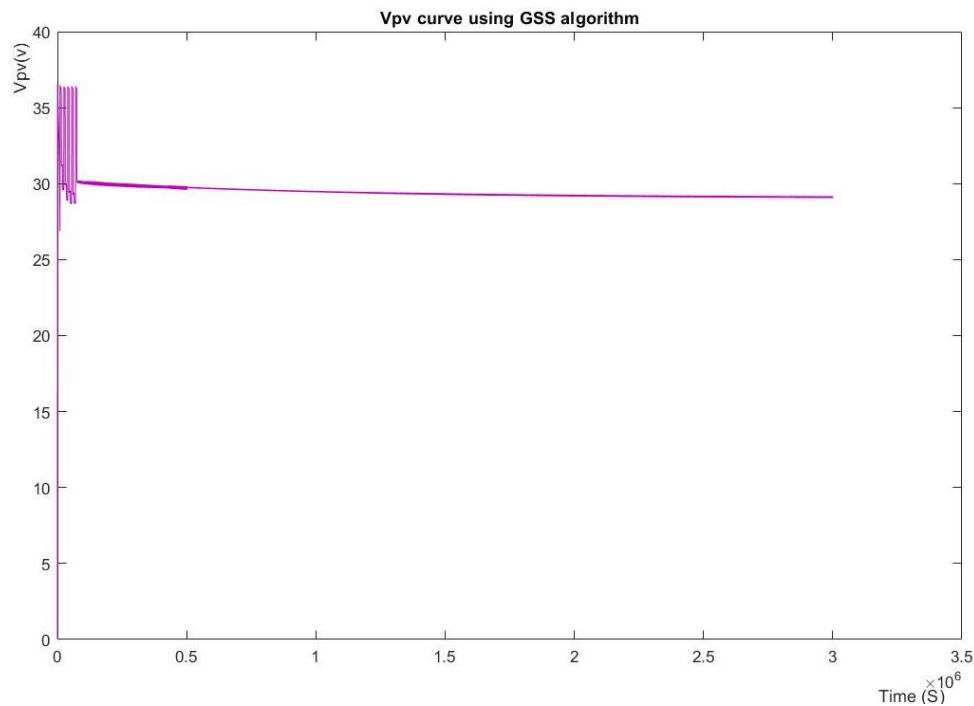


Figure 3.19: Voltage curve of single PV module under uniform conditions using GSS MPPT.

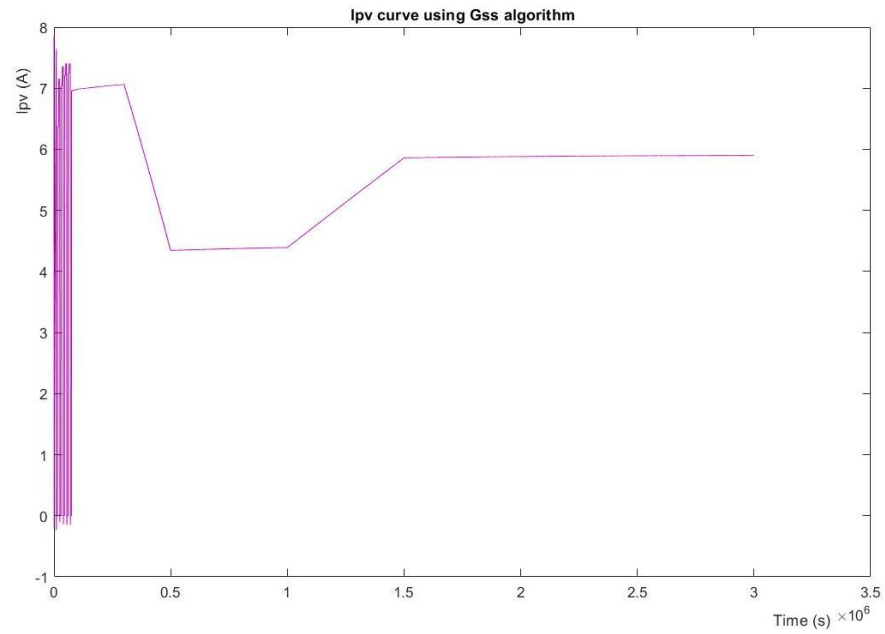


Figure 3.20: Current curve of single PV module under uniform conditions using GSS MPPT.

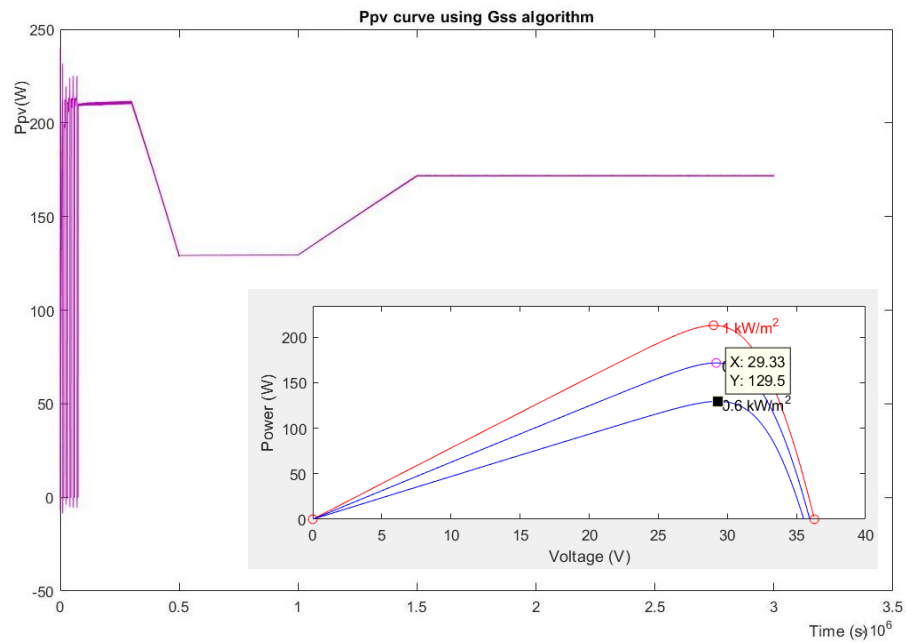


Figure 3.21: Power curve of single PV module under uniform conditions using GSS MPPT.

3.3.3.2- GSS MPPT for Five Series Modules- under uniform conditions:

Using the Simulink model shown in figure 3.12 we have changed the initial values as shown in table 3.4 with Gss function for 5 series modules with bypass diodes.

As in incremental conductance even in GSS we have used uniform irradiance and partial shading for the 5 series modules. In the uniform conditions the irradiance is the same as the one in table 3.3.

Figures 3.22 3.23 & 3.24 show the voltage current & power curves of 5 series modules under uniform irradiance using GSS Controller

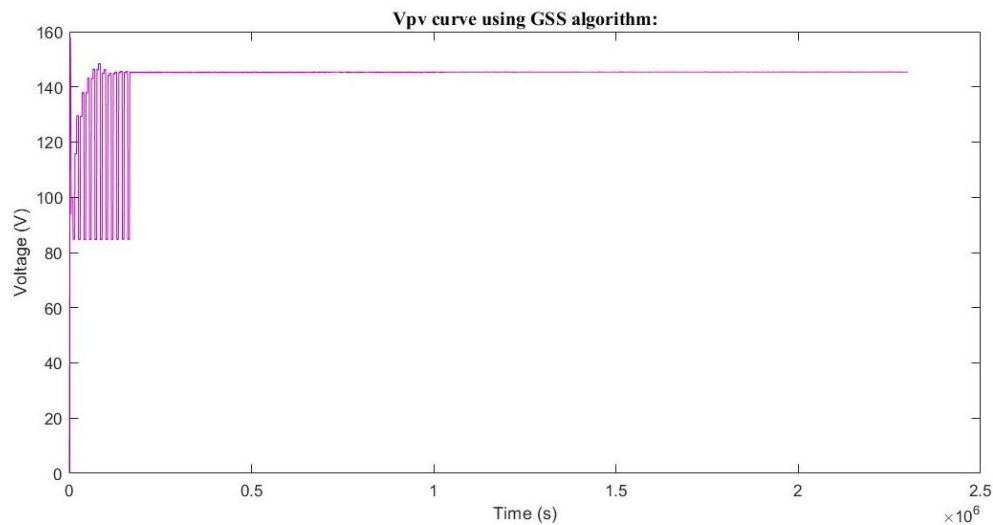


Figure 3.22: Voltage curve of five PV modules under uniform conditions using GSS MPPT.

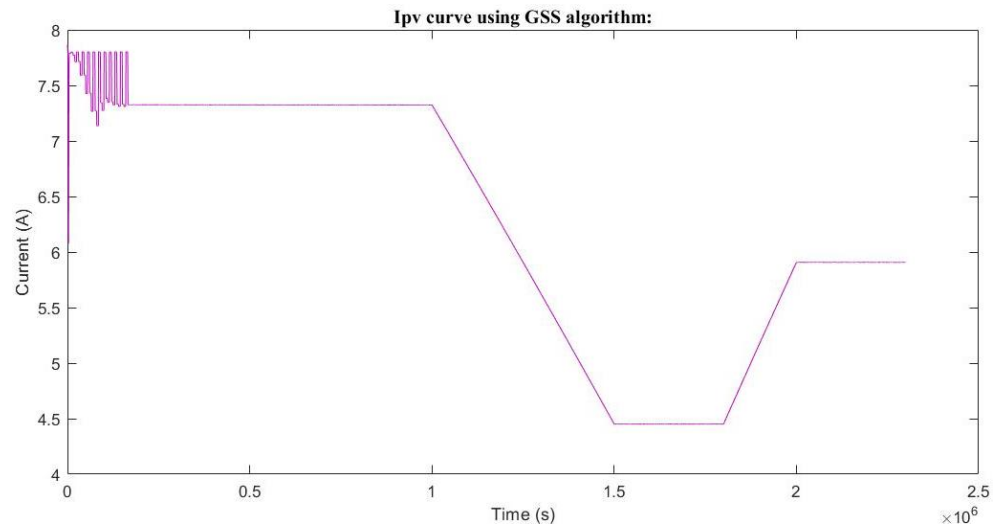


Figure 3.23: Current curve of five PV modules under uniform conditions using GSS MPPT.

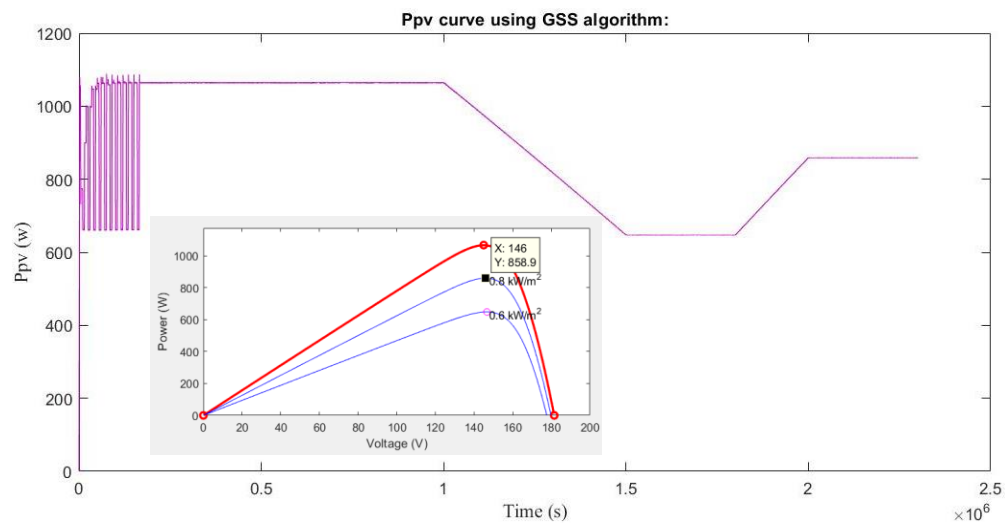


Figure 3.24: Power curve of five PV modules under uniform conditions using GSS MPPT.

3.3.3.3- GSS MPPT for Five Series Modules- under Shading conditions:

Figures 3.25 3.26 & 3.27 show the voltage current & power curves of 5 series modules under partial shading using GSS Controller

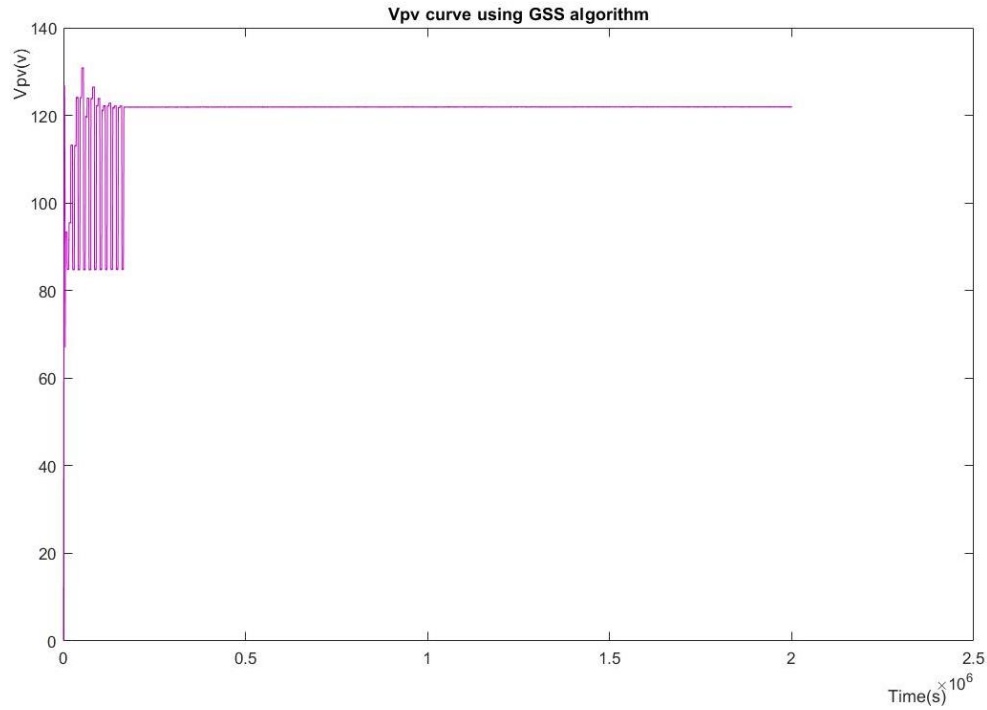


Figure 3.25: Voltage curve of five PV modules under partial shading conditions using GSS MPPT.

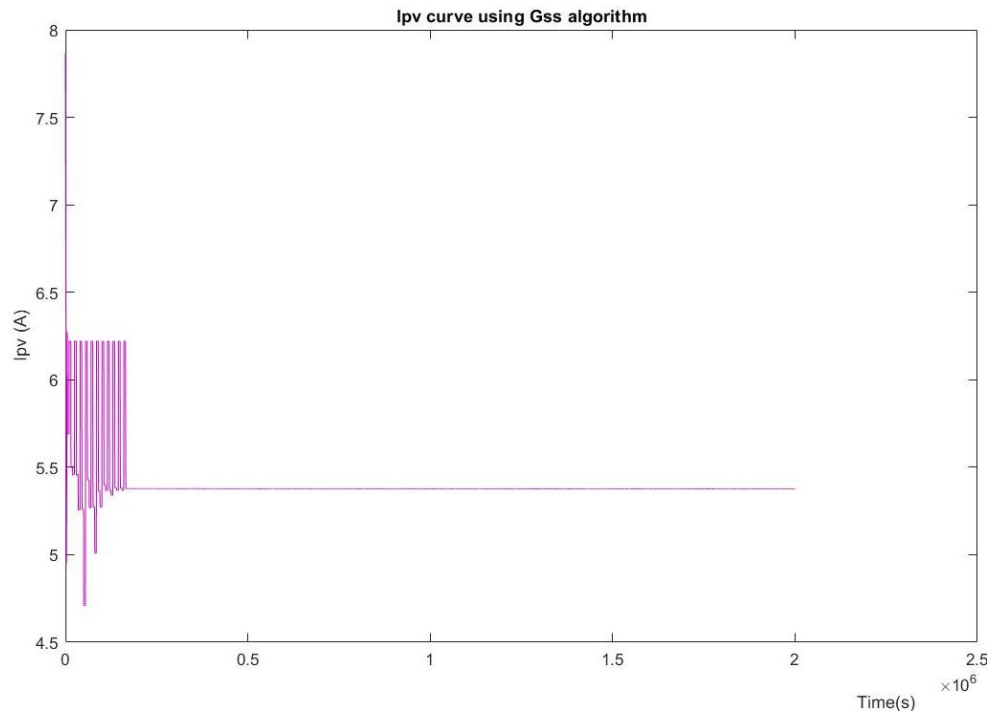


Figure 3.26: Current curve of five PV modules under partial shading conditions using GSS MPPT.

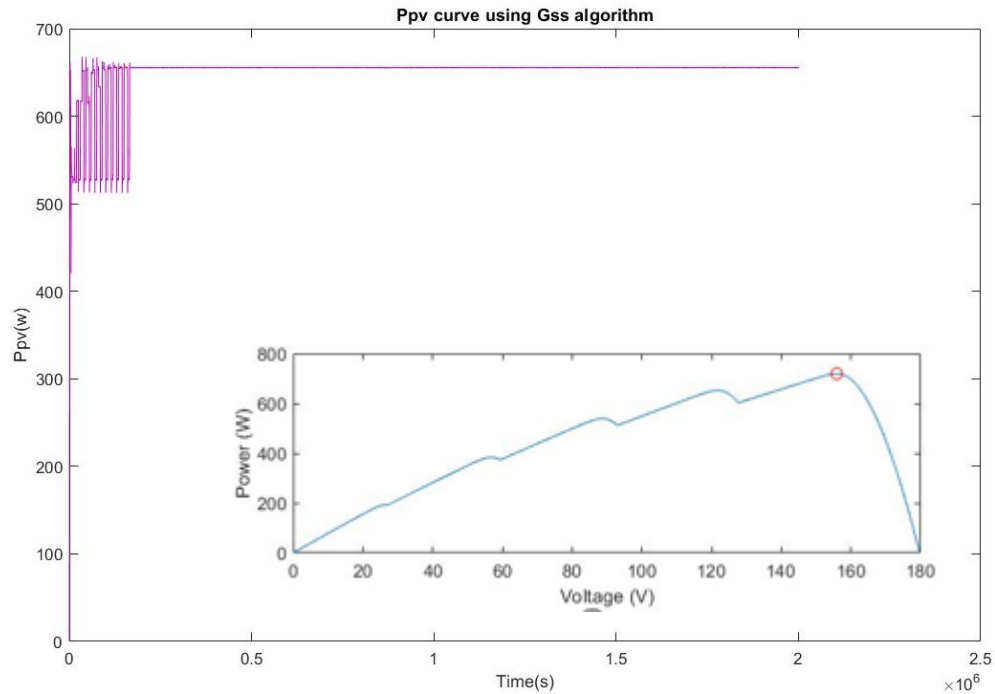


Figure 3.27: Power curve of five PV modules under partial shading conditions using GSS MPPT.

3.3.4 Particle Swarm Optimization PSO

3.3.4.1 PSO MPPT for a Single Module- under uniform conditions:

The third algorithm to be used is the PSO where it generates the duty cycle to be injected in the buck-boost we have initialized the PSO algorithm as shown in table 3.6

| Nbr of iterations | Swarm size | Intial duty cycle D | Initial velocity | Personal best of D | Global best of D |
|-------------------|------------|---------------------|---------------------------|--------------------|------------------|
| 5 | 3 | [0.2 0.5 0.8] | [0.001 0.001 0.001] | [0 0 0] | 0 |

Table 3.6: initialization parameters for a single module.

Table 3.7 shows the PSO based algorithm constants

| C1 | C2 | R1 | R2 | W(inertia) |
|-----|-----|--------|--------|------------|
| 1.2 | 1.6 | random | random | 0.4 |

Table 3.7: PSO Algorithm constants.

For the profile of the irradiance we have worked with 1000w/m² and 800 w/m²

Figures 3.28 3.29 & 3.30 show the voltage current & power curves of a single module under uniform irradiance using PSO Controller

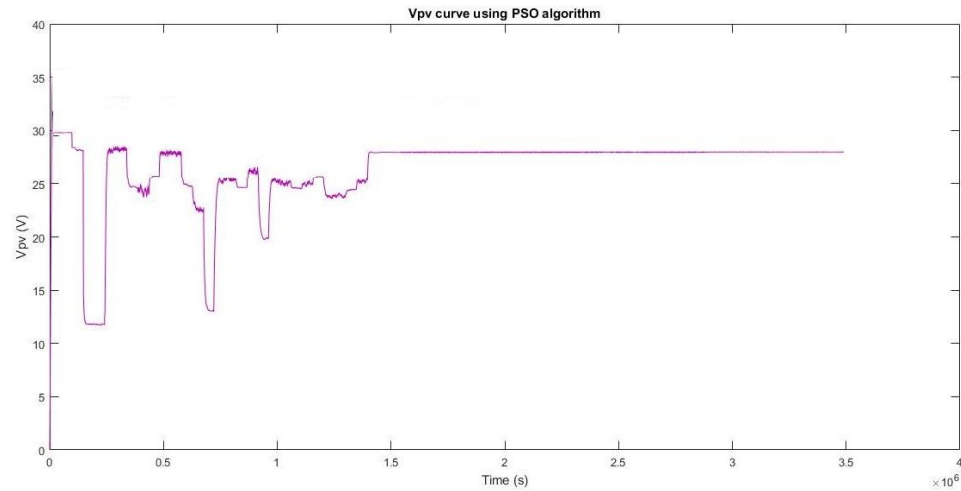


Figure 3.28: Voltage curve of single PV module under uniform conditions using PSO MPPT.

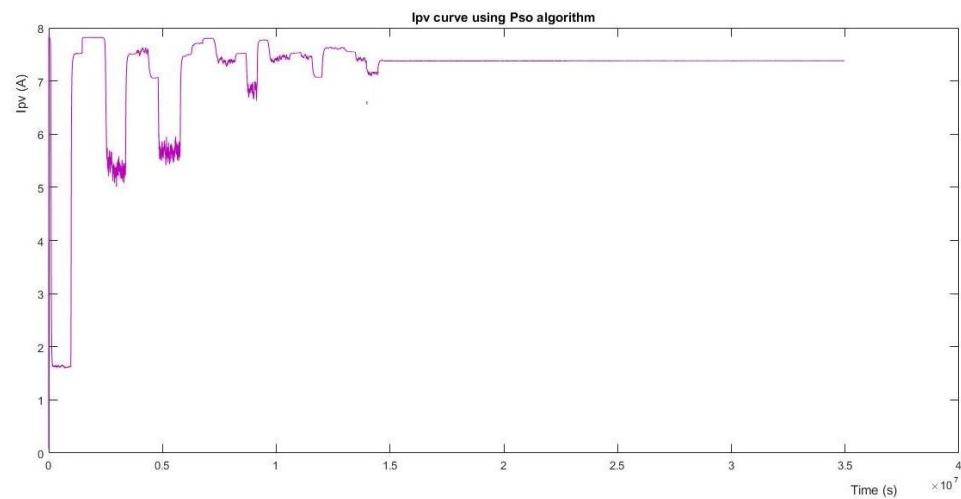


Figure 3.29: Current curve of single PV module under uniform conditions using PSO MPPT.

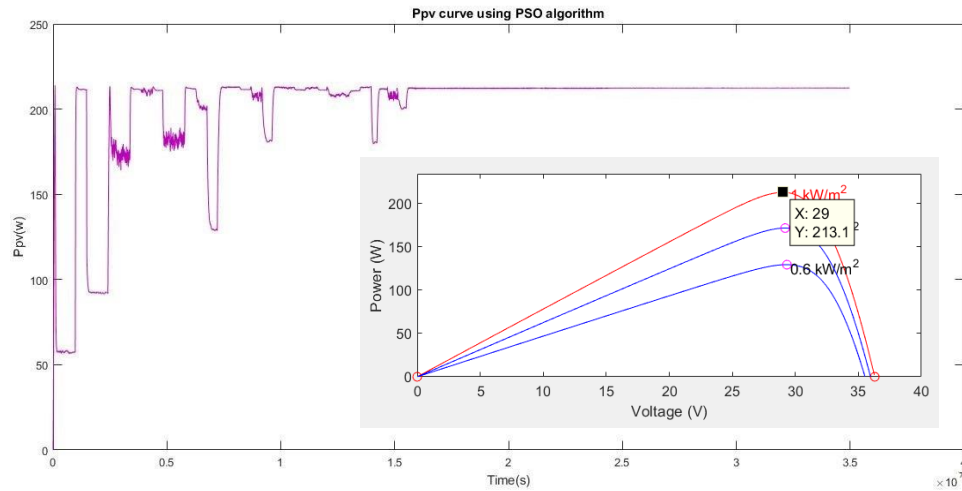


Figure 3.30: power curve of single PV module under uniform conditions using PSO MPPT.

3.3.4.2- PSO MPPT for Five Series Modules- under uniform conditions

The PSO algorithm takes a longer time to converge than GSS and Inc due to the multiple iterations it performs, therefore we have used only one normal condition for all PVs ($1000\text{w}/\text{m}^2$).

Figures 3.31 3.32 & 3.33 show the voltage current & power curves of 5 series modules under partial shading conditions using PSO Controller

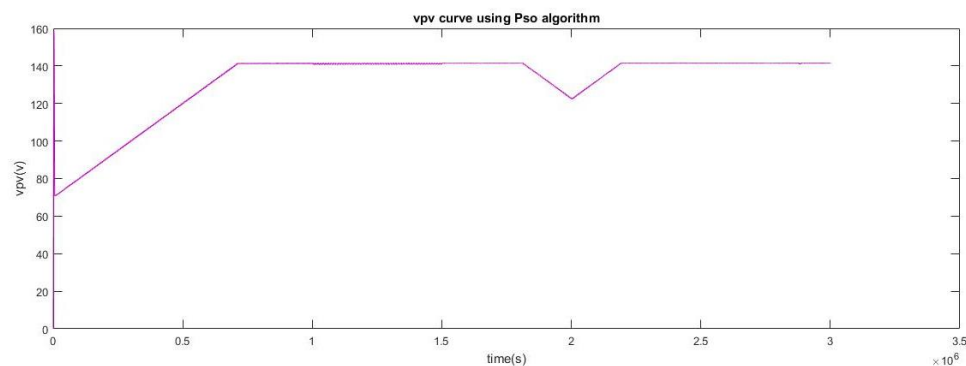


Figure 3.31: Voltage curve of five PV modules under uniform conditions using PSO MPPT.

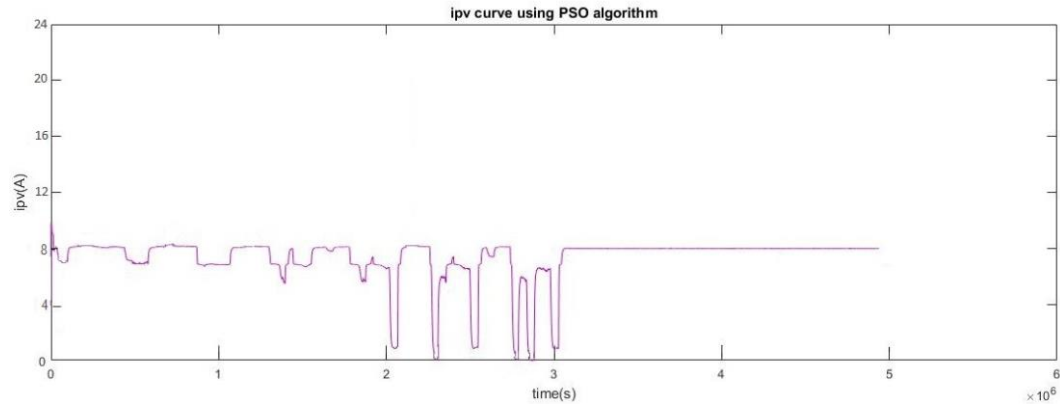


Figure 3.32: current curve of five PV modules under uniform conditions using PSO MPPT.

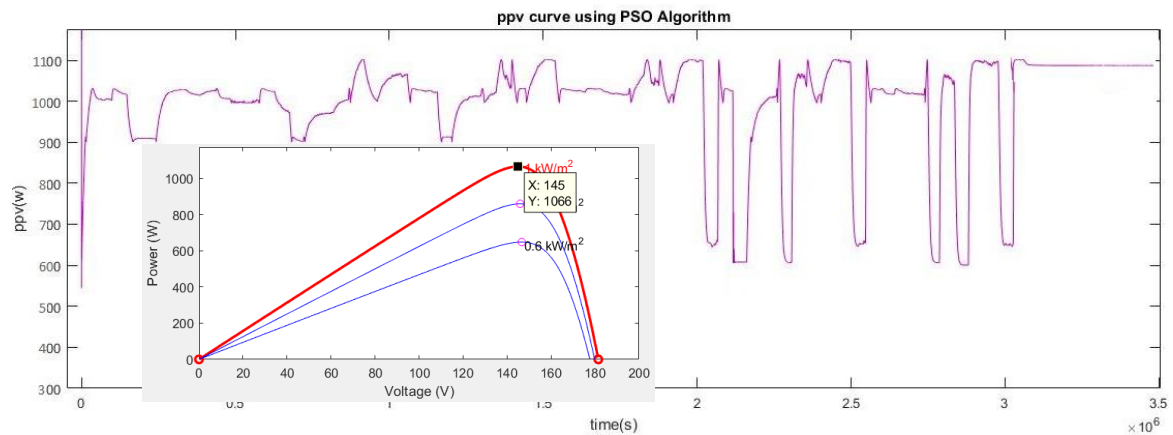


Figure 3.33: Power curve of five PV modules under uniform conditions using PSO MPPT.

3.3.4.3- PSO MPPT for Five Series Modules- under Shading conditions

For PSO algorithm we have kept the same partial shading conditions for incremental algorithm .

Figures 3.34 3.35 & 3.36 show the voltage current & power curves of 5 series modules under partial shading conditions using PSO Controller

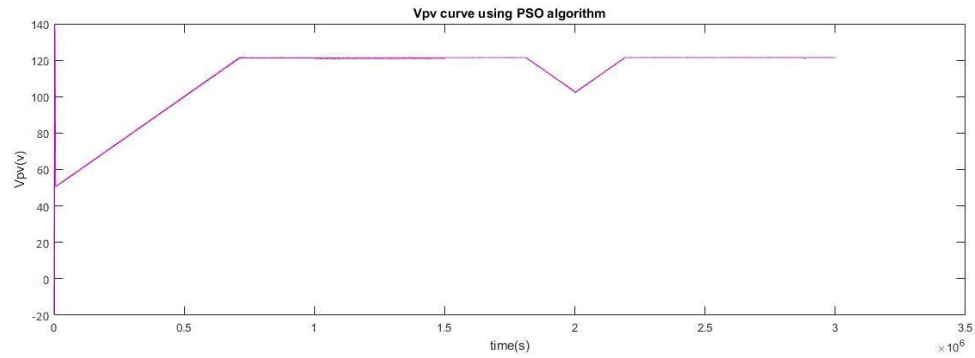


Figure 3.34: voltage curve of five PV modules under partial shading conditions using PSO MPPT.

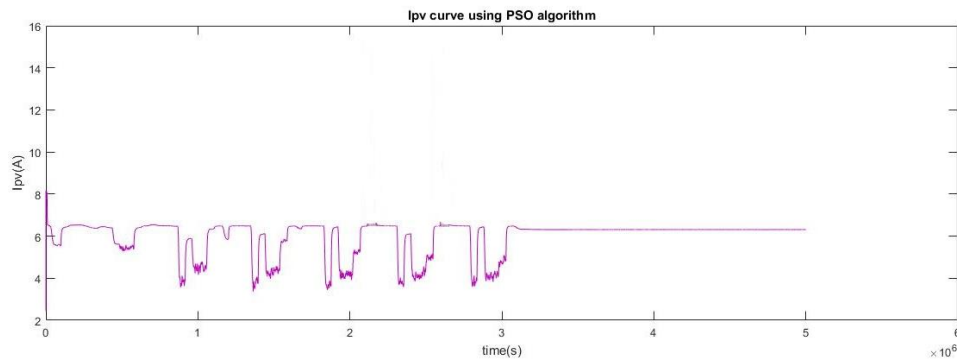


Figure 3.35: current curve of five PV modules under partial shading conditions using PSO MPPT.

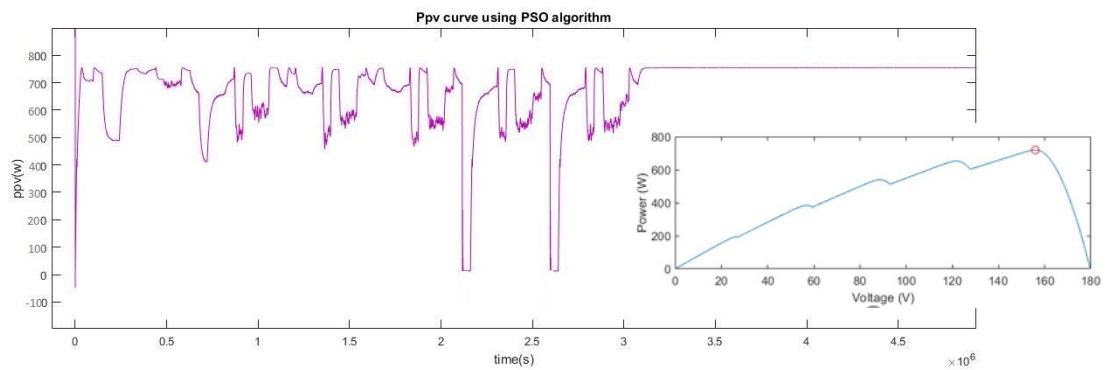


Figure 3.36: Power curve of five PV modules under partial shading conditions using PSO MPPT.

I

Under uniform irradiance:

- For single or multiple modules in series GSS and PSO oscillates, while searching for the MPP whereas InC does not oscillate.
- For single or multiple modules in series comparing the results of the three algorithms, we notice that all of them converges to the MPP, though GSS converges faster than incremental conductance and PSO which is the most time consuming.

Under shading condition:

- The three algorithms converged to different MPPTs:
the incremental conductance MPPT did not reach the global peak and converged to the third peak of figure 3.5 to the power value of 555W, the GSS MPPT also did not reach the global MPP though converged to the fourth peak of figure 3.5 to the value of 650 W, but PSO is the one which reached the global MPP since it converged to the fifth peak of the figure 3.5 to the value of 750W.
- The most efficient algorithm is the PSO since Inc and GSS did not converge to the GMPP.

3.4 Conclusion

In this chapter we have seen the performance of the PV system connected to a buck-boost converter, through the means of an MPPT tracker to control the buck and boost modes of the converter by obtaining the accurate duty cycle under normal conditions and partial shading conditions.

Incremental conductance, the golden section search, and the particle swarm optimization were used as MPPTs. Each algorithm was tested under normal and partial shading conditions. The most efficient algorithm was found to be the PSO, since it converged to the GMPP while neither algorithm did.

Chapter Four

Implementation and Discussion

4.1 Introduction

The final step of this project is the implementation part, we will implement the system described in the previous chapter, each part would be explained and illustrated. This work is divided into two parts: the control and power circuits, the control circuit consists of generating the gating signals for the control of the DC-DC converter, and the power circuit would consist of driver circuit for the MOSFET of the buck-boost converter, the PV array and finally the measurement circuit. We first test the characteristics of the PV module using a variable resistor, then we apply our algorithms in the control circuit to track the MPPT, the obtained results are discussed by the end.

4.2 Real PV characteristics

In order to test the performance of the whole system the characteristics of the PV panels, IV and PV curves, are necessary for the evaluation of the efficiency of the MPPT algorithm. For this purpose, we have connected the PV array to a variable resistor and recorded the values for I_{pv} and V_{pv} for multiple resistances at 9 am and at 16 pm, and finally plotted the correspondent IV and PV curves, a Volt-meter and an Ampere-meter are used for measurement purpose.

For the PV array we have connected five modules in series, and bypassed each module using a diode (1A). The parameters of the PV module are listed below:

- Type P-5 W
- Peak power (P_{max})=5W
- Open circuit voltage(V_{oc})=11.1V
- Maximum power voltage (V_{mp})=9.0V
- Short circuit current (I_{sc})=0.62A
- Maximum power current (I_{mp})=0.56A
- Maximum system voltage =1000 V
- Power tolerance = $\pm 3\%$
- Dimension (mm)=250*200*17

Figure 4.1 shows an image of the implemented circuit of PVs and variable resistor

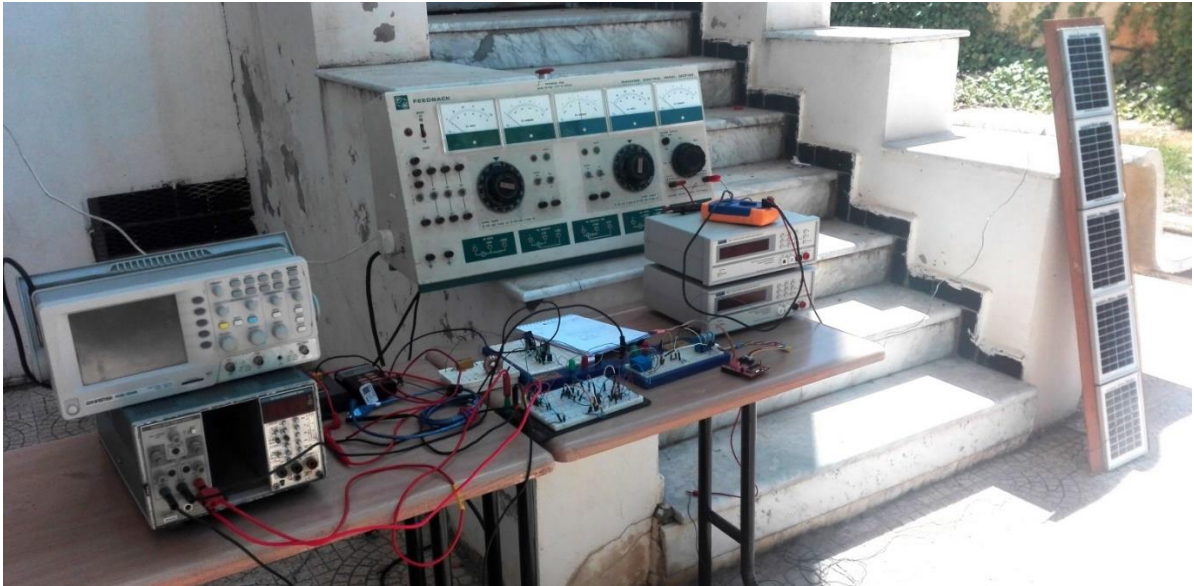


Figure 4.1: Overall system, Variable resistor and PVs connections

Table 4.1 shows the recorded values of I_{pv} and V_{pv} using a variable resistor at 9 am

| | | | | | | | | | | | | | | |
|----------|------|------|------|------|------|------|------|------|------|------|------|------|------|------|
| I_{pv} | 0,61 | 0,61 | 0,61 | 0,61 | 0,61 | 0,61 | 0,61 | 0,61 | 0,61 | 0,61 | 0,61 | 0,61 | 0,61 | 0,6 |
| V_{pv} | 1,8 | 2,8 | 3,3 | 4,4 | 5,5 | 6,3 | 6,6 | 8,2 | 9 | 10,2 | 11,7 | 13,8 | 15,4 | 17,4 |
| I_{pv} | 0,59 | 0,59 | 0,59 | 0,59 | 0,59 | 0,59 | 0,59 | 0,59 | 0,59 | 0,59 | 0,59 | 0,58 | 0,57 | 0,56 |
| V_{pv} | 20,3 | 21 | 22,9 | 26,5 | 27,2 | 28,5 | 29,9 | 32 | 34,2 | 36,4 | 37,3 | 38,3 | 39,4 | 40,2 |

| | | | | | | | | | | | | | | |
|----------|------|------|------|------|------|------|------|------|------|------|------|------|------|------|
| I_{pv} | 0,54 | 0,53 | 0,52 | 0,51 | 0,51 | 0,5 | 0,49 | 0,48 | 0,47 | 0,47 | 0,44 | 0,43 | 0,41 | 0,39 |
| V_{pv} | 40,7 | 41,4 | 41,9 | 42,3 | 42,6 | 42,9 | 43,3 | 43,7 | 43,8 | 44 | 44,7 | 45 | 45,3 | 45,8 |
| I_{pv} | 0,38 | 0,37 | 0,36 | 0,35 | 0,34 | 0,33 | 0,32 | 0,31 | 0,3 | 0,29 | 0,28 | 0,01 | | |
| V_{pv} | 46 | 46,2 | 46,4 | 46,6 | 46,7 | 47 | 47,1 | 47,2 | 47,3 | 47,4 | 47,6 | 50,9 | | |

Table 4.1: Recorded values for I_{pv} and V_{pv} at 9 am.

Figure 4.2 shows the obtained curves for IV and PV characteristics for a variable resistor at 9 am

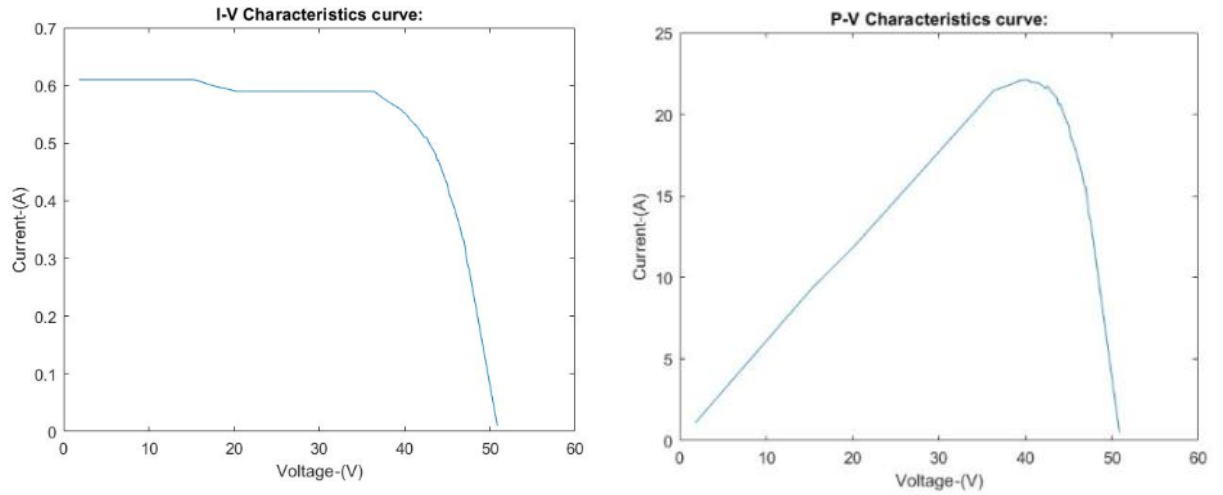


Figure 4.2: IV and PV characteristics at 9 am.

Table 4.2 shows the recorded values of I_{pv} and V_{pv} using a variable resistor at 4pm

| | | | | | | | | | | |
|----------|-------|-------|--------|--------|-------|-------|--------|--------|--------|--------|
| I_{pv} | 0.57 | 0.57 | 0.5695 | 0.567 | 0.566 | 0.564 | 0.5635 | 0.563 | 0.562 | 0.559 |
| V_{pv} | 0.41 | 0.65 | 0.9 | 2.4 | 4.3 | 7.6 | 11.3 | 14.7 | 16.3 | 18.2 |
| I_{pv} | 0.558 | 0.556 | 0.554 | 0.553 | 0.552 | 0.55 | 0.549 | 0.5462 | 0.5449 | 0.5436 |
| V_{pv} | 22.8 | 30 | 31.62 | 34.269 | 36.36 | 37.14 | 38.85 | 38.98 | 39.5 | 40.3 |

| | | | | | | | | | | |
|----------|--------|--------|------|-------|------|-------|-------|-------|------|--------|
| I_{pv} | 0.5428 | 0.5415 | 0.54 | 0.517 | 0.5 | 0.48 | 0.467 | 0.45 | 0.41 | 0.39 |
| V_{pv} | 40.74 | 41.35 | 42.3 | 43.2 | 43.6 | 43.71 | 44.21 | 45.53 | 45.8 | 46.3 |
| I_{pv} | 0.32 | 0.29 | 0.25 | 0.22 | 0.2 | 0.18 | 0.11 | 0.07 | 0.02 | 0.0003 |
| V_{pv} | 46.9 | 47.3 | 47.7 | 48.2 | 48.5 | 48.7 | 49.1 | 49.3 | 49.8 | 50.1 |

Table 4.2: recorded values for I_{pv} and V_{pv} at 4 pm.

Figure 4.3 shows the obtained curves for IV and PV characteristics for a variable resistor at 4 pm

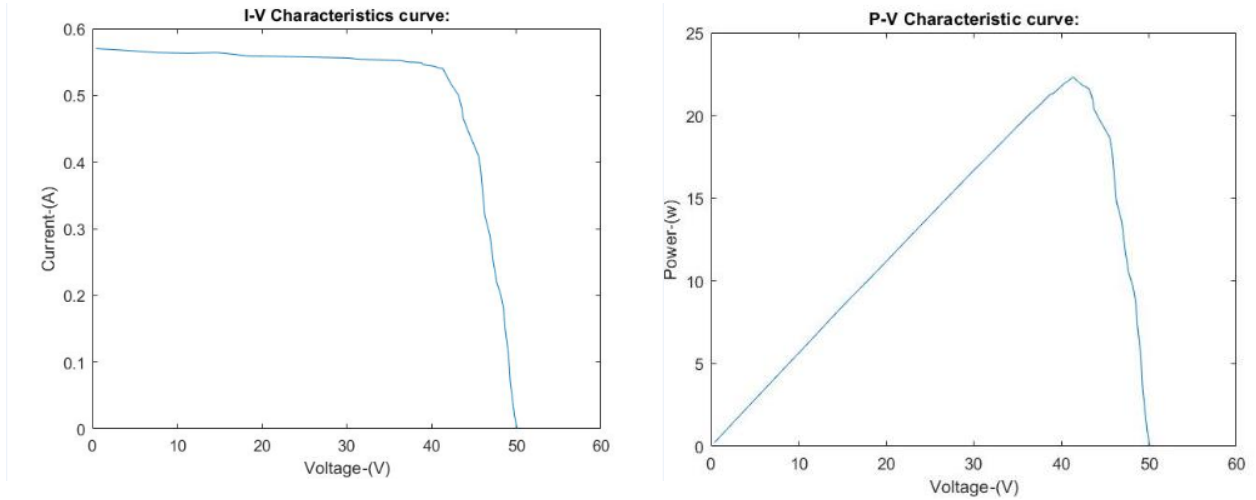


Figure 4.3: IV and PV characteristics at 4pm.

4.3 The Implemented System

The whole implemented system is consisting of: the power circuit, measurement circuit and the control circuit. The power circuit consists of: the PV panels supplying a resistive load ($R=250\Omega$ - 25W) through the buck-boost dc-dc converter, the voltage and current of the PV panels are obtained using the voltage and current sensors. The control circuit is built in the Simulink, it consist of: the DSP receiving the measured voltage and current as inputs through ADC input ports (ADCIN A0- ADCIN A1) initialized to operate as analog to digital converters , running the MPPT algorithm , and generating the PWM pulses to be injected as inputs to the gate driver circuit with a frequency of 5 KHz through PWM output ports (EPWM1A-EPWM1B).

4.3.1- Measurement devices and circuit

To track the MPPT by finding the power we need to measure the output current I_{pv} and output voltage V_{pv} from the PV panel

4.3.1.a- Current sensor:

The DSP (microcontroller) works within a voltage range of (0-3.3v) therefore we cannot implement I_{pv} directly in the DSP, so we need to convert it to voltage using resistors. LA 55-P LEM HALL Effect current sensor has been used to measure I_{pv} by supplying it with $\pm 15V$ and measuring through a resistor $R_m = 100\Omega$

Figure 4.4 shows the LA 55-P connection to the DSP input

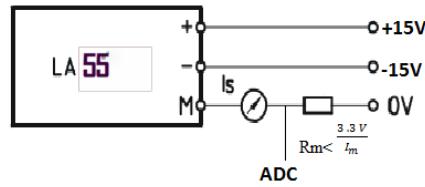


Figure 4.4: the LA 55-P connection.

4.3.1.b- Voltage sensor:

The voltage sensor used is the Voltage Transducer LV 25-P , which works with 10mA input current and 25mA output current , we have used a Total resistor of $R_T = 6K\Omega$ to obtain a current of 10 mA and a measurement resistor $R_m = 100$, the output of the sensor is connected to the DSP .

Figure 4.5 shows the LV 25-P connection to the DSP input

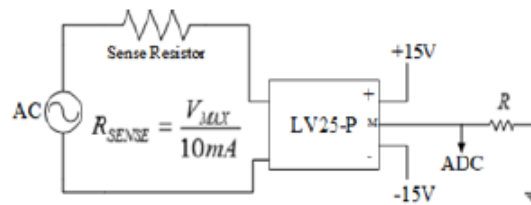


Figure 4.5: the LV 25-P connection.

Figure 4.6 shows an image of the implementation of the measurement circuitry

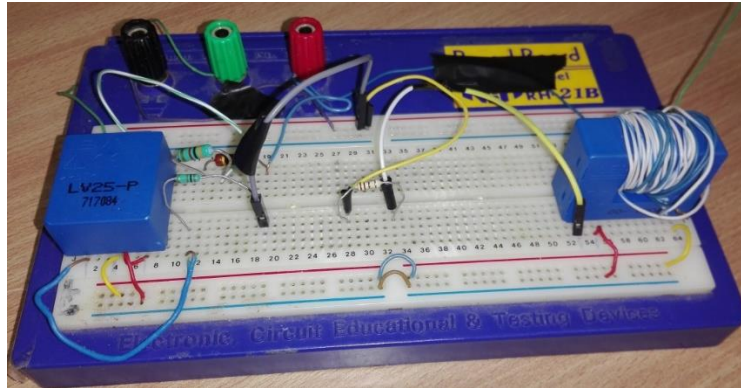


Figure 4.6: measurement circuit.

4.4 Switching elements

Nowadays power electronic elements are widely used to control the different parameters of a certain circuit, among power electronics we find the switches such as MOSFET, BJTS, IGBTs GTO...etc. These switches are generally used to implement the DC-DC converters and controlled by gating signals. There are current controlled devices and voltage-controlled devices, but voltage-controlled devices are preferred. Among these devices the most used are FET and IGBT, where MOSFET have fast switching time and a wide range of voltage and current used generally in choppers; on the other hand, IGBTs have a low frequency and are found exclusively in inverters. Due to the high frequency range of MOSFET we have chosen this component for our implementation.

4.4.1- Gate drive circuit for MOSFET

We are working with a non-inverting buck boost converter; therefore, we need to supply the gate of two different MOSFET that would be working in a complementary state allowing the buck and boost modes to operate separately. The DSP controller works in a range of (0-3.3V) however the required gate voltage signals to drive the MOSFET attain 15V. For this purpose a power amplifier & insulator circuit is implemented, to amplify the input voltage from the DSP and to protect the DSP from any damage.

Figure 4.7 shows the schematic of the gate driver circuit using an optocoupler

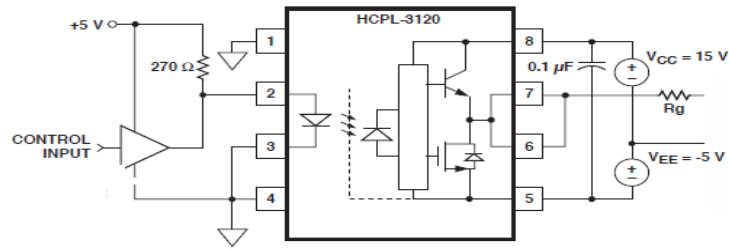


Figure 4.7 schematic of the gate driver circuit.

The control output from the DSP is an input to a buffer to amplify it to 5V then inject it to the HCNW3120 optocoupler.

Figure 4.8 shows an image of the implementation of the gate driver for both MOSFET

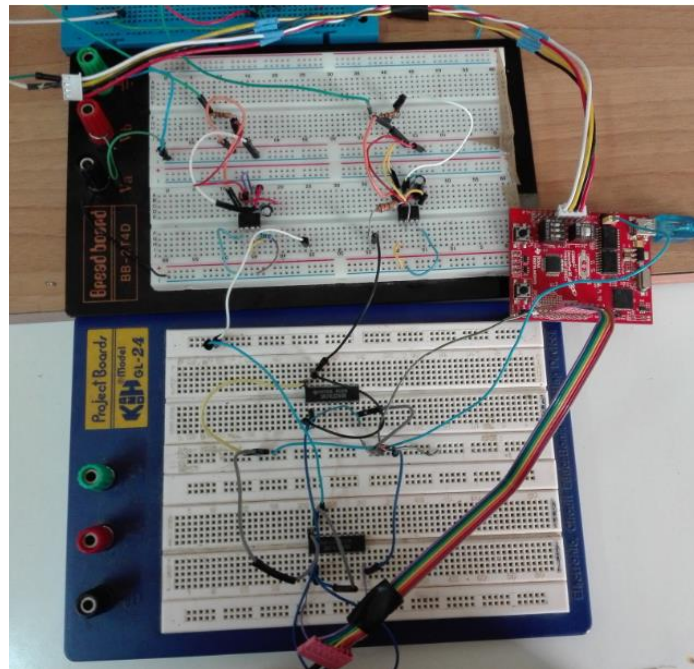


Figure 4.8: Gate driver implementation.

The buck-boost converter was implemented, and tested with a DC-supply as a source and a constant duty cycle obtained from the PWM port of the DSP.

Figure 4.9 shows the image the implementation of the buck boost converter

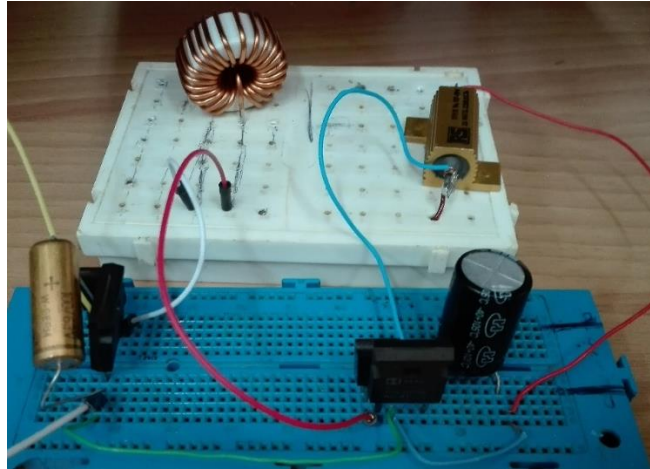


Figure 4.9: DC-DC Buck-Boost converter.

In order to test the buck boost converter performance, we assumed a duty cycle

$d = 0.2$ which would lead to 40% ON gate of boost switch, and 60% OFF of the buck switch. That is the output for MOSFET gates control.

Figure 4.10 shows the Simulink model for setting the buck boost.

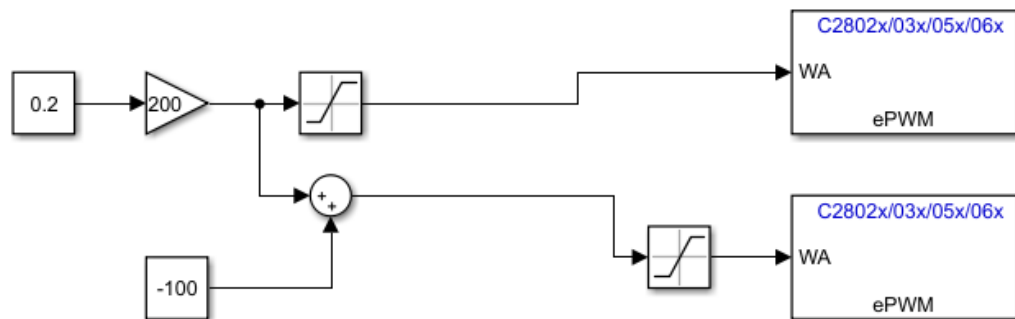


Figure 4.10: Simulink model for setting the buck boost.

Figure 4.11 shows the obtained PWM pulses from the DSP by assuming duty cycle

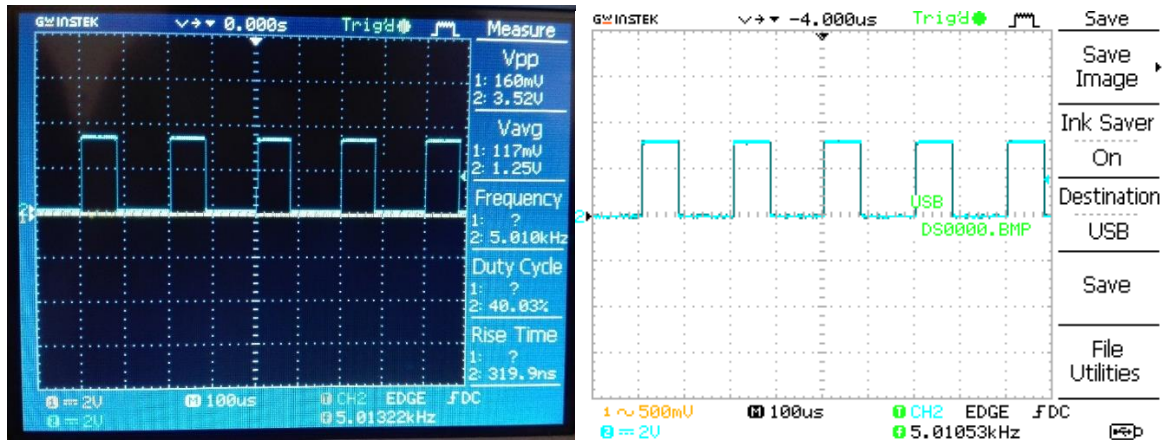


Figure 4.11.a: obtained PWM pulses from the DSP by assuming duty cycle

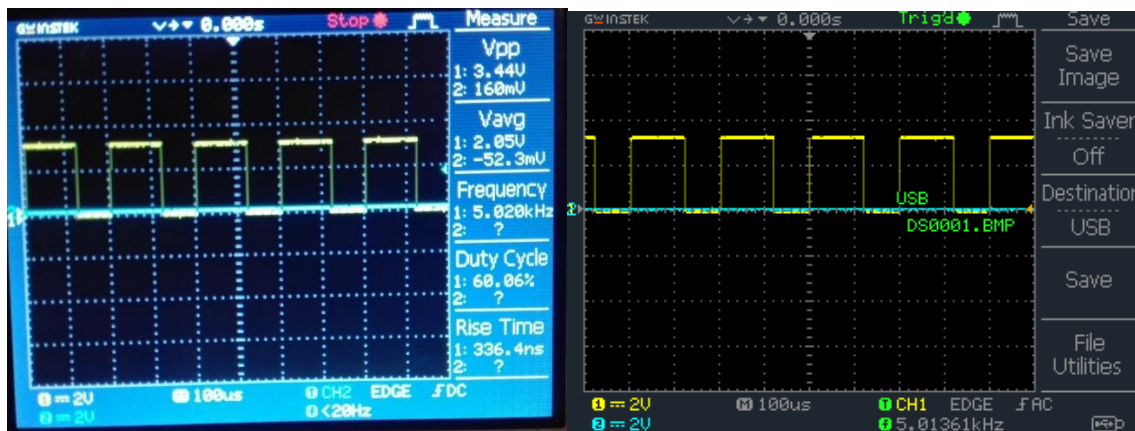


Figure 4.11.b: obtained PWM pulses from the DSP by assuming duty cycle

Figure 4.12 shows the Simulink model for obtaining PWM pulses from the DSP with receiving V_{pv} and I_{pv} from PV panels

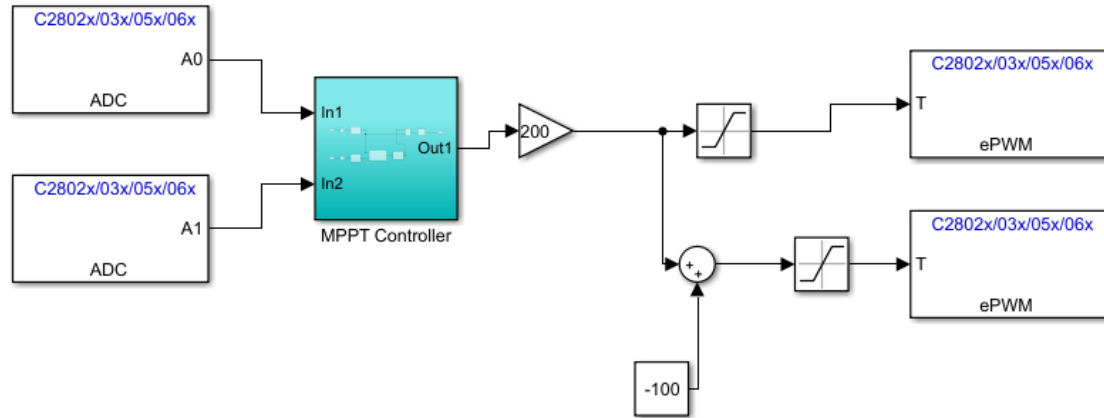


Figure 4.12: Control circuit.

Figure 4.13 shows the overall implemented system

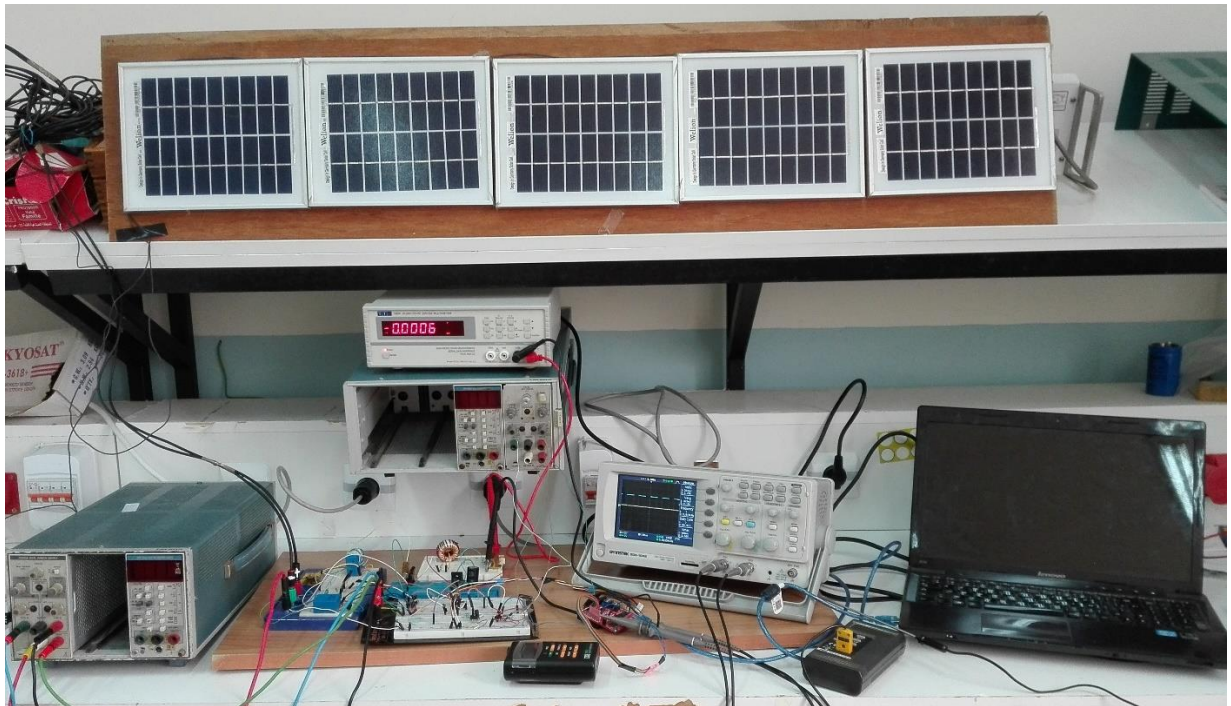


Figure 4.13: Overall system.

4.5 Discussion:

- From figures 4.2 and 4.3 we notice that the IV and PV curves obtained at different times of the day (9am-4pm) are slightly different due to the effect of the irradiance on the PV array, these results confirm the theoretical ones discussed in the previous chapters.
- From figure 4.10 or figure 4.12; the duty cycle obtained from the MPPT is an input to a comparator, two PWM signals are obtained shown in figures 4.11a 4.11b, one is a pulse with 3.3V average value and the second one is 0V alternatively, these two signals are responsible of the operation of the buck and boost modes separately.
- Due to the lack of good components ,the drive circuit did not operate quiet well ,since the pulse signals obtained from the DSP are distorted when injected through the gate drive circuit, this problem prevented us from reaching the final step of our implementation for obtaining the final results after running the three algorithms INC, GSS and PSO.

4.6 Conclusion

In this chapter the different steps and methodology for the design and the implementation of MPPT system are covered. First the power circuit is constructed, the PV array is implemented using five modules as in the simulation part discussed in chapter three and tested to obtain it's characteristics, the measurement circuit is implemented using voltage and current sensors, Next the control unit is designed based on DSP microcontroller; its pulses are injected in the circuit of the gate driver . Finally, the whole system was implemented using all of the above mentioned apparatus, but the results did not satisfy the theoretical part due to the defected components.

Conclusion

General conclusion

The presented project dealt with the analysis, simulation, design, and implementation of a maximum power point tracker for a standalone photovoltaic system, using DSP C2000.

The aim of this work was to track the maximum power point of a PV array, to maximize its efficiency using a conventional algorithm such as the incremental conductance; and new algorithms such as the golden section search, and particle swarm optimization. These algorithms were tested and simulated in MATLAB/SIMULINK software, implemented in C2000 DSP microcontroller, and finally used in the PV system, where the PV array is connected to a buck-boost converter which supplies a load.

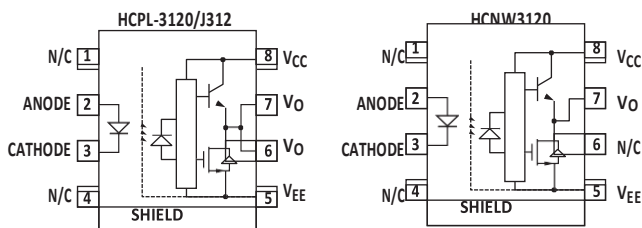
Since the irradiance tends to vary and cannot be kept constant, the voltage across the load supplied by the PV system must be kept constant. Therefore, a buck boost converter was chosen to either increase the voltage or decrease it, depending on the specific value of the duty cycle obtained from the MPPT. Each technique was tested under normal and partial shading conditions to specify its efficiency when generating the appropriate duty cycle. Simulation results have shown the effectiveness of PSO in tracking the MPP under uniform and non-uniform irradiance conditions.

The simulation and the implementation parts work with different PV arrays parameters, due to the non-availability of the equipment in the laboratory; the buck-boost converter was simulated with the values of components available to obtain accurate results in the implementation part.

This thesis provides the guidelines for designing a simple MPPT module. Improvements in the design provided can be made in optimizing the real conditions using an emulator to provide a scoped study.

HCPL-3120/J312, HCNW3120**2.5 Amp Output Current IGBT Gate Drive Optocoupler****Data Sheet****Description**

The HCPL-3120 contains a GaAsP LED while the HCPL-J312 and the HCNW3120 contain an AlGaAs LED. The LED is optically coupled to an integrated circuit with a power output stage. These optocouplers are ideally suited for driving power IGBTs and MOSFETs used in motor control inverter applications. The high operating voltage range of the output stage provides the drive voltages required by gate controlled devices. The voltage and current supplied by these optocouplers make them ideally suited for directly driving IGBTs with ratings up to 1200 V/100 A. For IGBTs with higher ratings, the HCPL-3120 series can be used to drive a discrete power stage which drives the IGBT gate. The HCNW3120 has the highest insulation voltage of $V_{IORM} = 1414 V_{peak}$ in the IEC/EN/DIN EN 60747-5-5. The HCPL-J312 has an insulation voltage of $V_{IORM} = 1230 V_{peak}$ and the $V_{IORM} = 630 V_{peak}$ is also available with the HCPL-3120 (Option 060).

Functional Diagram**Features**

- 2.5 A maximum peak output current
- 2.0 A minimum peak output current
- 25 kV/ μ s minimum Common Mode Rejection (CMR) at $V_{CM} = 1500 V$
- 0.5 V maximum low level output voltage (V_{OL})
Eliminates need for negative gate drive
- $I_{CC} = 5$ mA maximum supply current
- Under Voltage Lock-Out protection (UVLO) with hysteresis
- Wide operating V_{CC} range: 15 to 30Volts
- 500 ns maximum switching speeds
- Industrial temperature range: $-40^{\circ}C$ to $100^{\circ}C$
- SafetyApproval:

UL Recognized

3750 Vrms for 1 min. for HCPL-3120/J312

5000 Vrms for 1 min. for HCNW3120

CSA Approval**IEC/EN/DIN EN 60747-5-5 Approved:**

$V_{IORM} = 630 V_{peak}$ for HCPL-3120 (Option 060)

$V_{IORM} = 1230 V_{peak}$ for HCPL-J312

$V_{IORM} = 1414 V_{peak}$ for HCNW3120

TRUTH TABLE

| LED | $V_{CC} - V_{EE}$ "POSITIVE GOING" (i.e., TURN-ON) | $V_{CC} - V_{EE}$ "NEGATIVE GOING" (i.e., TURN-OFF) | V_o |
|-----|--|---|------------|
| OFF | 0 - 30 V | 0 - 30 V | LOW |
| ON | 0 - 11 V | 0 - 9.5 V | LOW |
| ON | 11 - 13.5 V | 9.5 - 12 V | TRANSITION |
| ON | 13.5 - 30 V | 12 - 30 V | HIGH |

SN74LS240, SN74LS244

Octal Buffer/Line Driver with 3-State Outputs

The SN74LS240 and SN74LS244 are Octal Buffers and Line Drivers designed to be employed as memory address drivers, clock drivers and bus-oriented transmitters/receivers which provide improved PC board density.

- Hysteresis at Inputs to Improve Noise Margins
- 3-State Outputs Drive Bus Lines or Buffer Memory Address Registers
- Input Clamp Diodes Limit High-Speed Termination Effects

GUARANTEED OPERATING RANGES

| Symbol | Parameter | Min | Typ | Max | Unit |
|----------|-------------------------------------|------|-----|------|------|
| V_{CC} | Supply Voltage | 4.75 | 5.0 | 5.25 | V |
| T_A | Operating Ambient Temperature Range | 0 | 25 | 70 | °C |
| I_{OH} | Output Current – High | | | -3.0 | mA |
| | | | | -15 | mA |
| I_{OL} | Output Current – Low | | | 24 | mA |

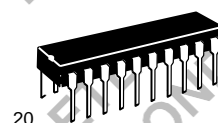


ON Semiconductor

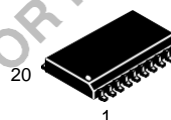
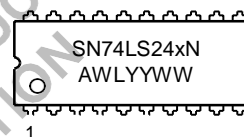
<http://onsemi.com>

LOW
POWER
SCHOTTKY

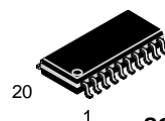
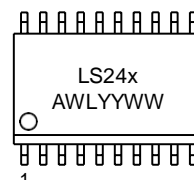
MARKING DIAGRAMS



PDIP-20
N SUFFIX
CASE 738



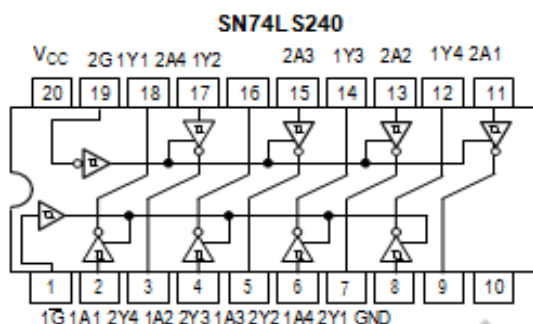
SOIC-20
DW SUFFIX
CASE 751D



SOEIAJ-20
M SUFFIX
CASE 967

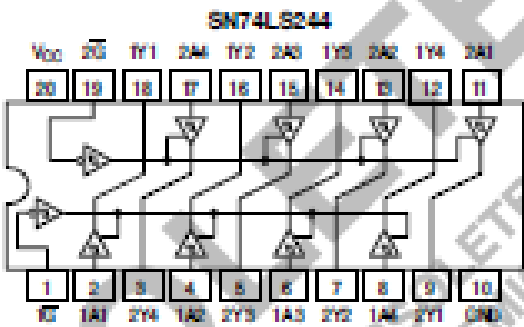
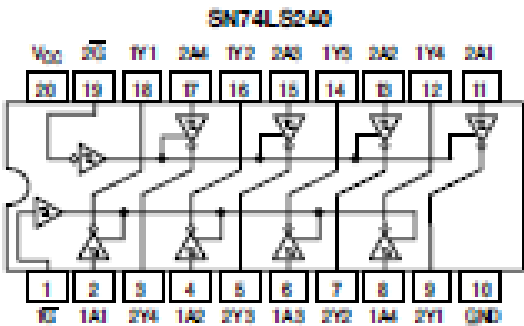


LOGIC AND CONNECTION DIAGRAMS DIP (TOP VIEW)



SN74LS240, SN74LS244

LOGIC AND CONNECTION DIAGRAMS DIP (TOP VIEW)



TRUTH TABLES

SN74LS240

| INPUTS | | OUTPUT |
|--------|---|--------|
| 1G, 2G | D | |
| L | L | H |
| L | H | L |
| H | X | (Z) |

SN74LS244

| INPUTS | | OUTPUT |
|--------|---|--------|
| 1G, 2G | D | |
| L | L | L |
| L | H | H |
| H | X | (Z) |

H = HIGH Voltage Level
L = LOW Voltage Level
X = Indeterminate
Z = HIGH Impedance

Appendix D: DSP TMS320f28027f

S

| Mux Value | | | | | | Mux Value | | | |
|-----------------|--------------------|-------------------|-----------|--------|--------|-----------|-------------------|--------------------|-----------------|
| 3 | 2 | 1 | 0 | J1 Pin | J5 Pin | 0 | 1 | 2 | 3 |
| | | | +3.3V | 1 | 1 | +5V | | | |
| | | | ADCINA6 | 2 | 2 | GND | | | |
| TZ2 | SDAA | SCIRXDA | GPIO28 | 3 | 3 | ADCINA7 | | | |
| TZ3 | SCLA | SCITXDA | GPIO29 | 4 | 4 | ADCINA3 | | | |
| Rsvd | Rsvd | COMP2OUT | GPIO34 | 5 | 5 | ADCINA1 | | | |
| | | | ADCINA4 | 6 | 6 | ADCINA0 | | | |
| | SCITXDA | SPICLK | GPIO18 | 7 | 7 | ADCINB1 | | | |
| | | | ADCINA2 | 8 | 8 | ADCINB3 | | | |
| | | | ADCINB2 | 9 | 9 | ADCINB7 | | | |
| | | | ADCINB4 | 10 | 10 | NC | | | |
| 3 | 2 | 1 | 0 | J6 Pin | J2 Pin | 0 | 1 | 2 | 3 |
| Rsvd | Rsvd | EPWM1A | GPIO0 | 1 | 1 | GND | | | |
| COMP1OUT | Rsvd | EPWM1B | GPIO1 | 2 | 2 | GPIO19 | SPISTEA | SCIRXDA | ECAP1 |
| Rsvd | Rsvd | EPWM2A | GPIO2 | 3 | 3 | GPIO12 | TZ1 | SCITXDA | Rsvd |
| COMP2OUT | Rsvd | EPWM2B | GPIO3 | 4 | 4 | NC | | | |
| Rsvd | Rsvd | EPWM3A | GPIO4 | 5 | 5 | RESET# | | | |
| ECAP1 | Rsvd | EPWM3B | GPIO5 | 6 | 6 | GPIO16/32 | SPISIMOA/ SDAA | Rsvd/ EPWMSYNCl | TZ2/ ADCSOCA |
| TZ2/ ADCSOCA | Rsvd/ EPWMSYNCl | SPISIMOA/ SDAA | GPIO16/32 | 7 | 7 | GPIO17/33 | SPISOMIA/ SCLA | Rsvd/ EPWMSYNCO | TZ3/ ADCOCB |
| TZ3/ ADCOCB | Rsvd/ EPWMSYNCO | SPISOMIA/ SCLA | GPIO17/33 | 8 | 8 | GPIO6 | EPWM4A | EPWMSYNCl | EPWMSYNCO |
| | | | NC | 9 | 9 | GPIO7 | EPWM4B | SCIRXDA | Rsvd |
| | | | NC | 10 | 10 | ADCINB6 | | | |

Table D.1: Pins' location on the DSP TMS320f28027f

REFERENCES

- [1]. Energy kids, Us Energy information administration “Solar Basics” found available online <http://www.eia.doe.gov/kids/energyfacts/sources/renewable/solar.html>
- [2]. B.K. Bose, P.M. Szczeny, and R.L. Steigerwald, “Microcomputer control of a residential photovoltaic power conditioning system” IEEE Transactions on Industrial Electronics, Vol. IA-21, 1182-1191, Sept./Oct. 1985.
- [3]. Yusof, Y.; Sayuti, S.H.; Abdul Latif, M.; Wanik, M.Z.C. “Modeling and simulation of maximum power point tracker for photovoltaic system”. In Proceedings of Power and Energy Conference, Kuala Lumpur, Malaysia, November, 29–30, 2004; 88–93.
- [4]. Wang, Y.J and Hsu, P.C. “Analytical modelling of partial shading and different orientation of photovoltaic modules”. Renewable. Power IET **2010**, 4, 272–282.
- [5]. Kajihara, A. and Harakawa, A.T.” Model of photovoltaic cell circuits under partial shading”. In Proceedings of IEEE International Conference on Industrial Technology (ICIT), Hong Kong, China, December 14–17 2005; 866–870.
- [6]. Pandiarajan, N. and Muthu, R. “Mathematical modeling of photovoltaic module with Simulink”. In Proceedings of the 1st International Conference on Electrical Energy Systems (ICEES), Newport Beach, CA, USA, January 3–5, 2011; 258–263.
- [7]. Durgadevi, A; Arulselvi, S and Natarajan, S.P. “Photovoltaic modeling and its characteristics”. In Proceedings of International Conference on Emerging Trends in Electrical and Computer Technology (ICETECT), 23–24 March 2011; 469–475.
- [8]. Energies open access journals available online <http://www.mdpi.com/journal/energies>, 21st June, 2019.
- [9]. Hatim Diab “Intelligent Maximum Power Tracking and Inverter Hysteresis Current Control of Grid-connected PV Systems”. In proceedings of the International Conference on Advances in Power Conversion and Energy Technologies, INDIA APCET- 2012.
- [10]. Silvestre, S.; Boronat, A. and Chouder, A. “Study of bypass diodes configuration on PV modules”. Application energy 2009, 1632–1640.
- [11]. Mohammad Mehdi; Seyed Mahmoudian; Saad Mekhilef, Rasoul Rahmani, Rubiyah Yusof and Ehsan Taslimi Renani “Integration of Large-Scale Photovoltaic system in the distribution grid under partially shading”. In proceedings of the international conference on electrical sciences and technologies, CISTEM, Maghreb 2014.
- [12]. Saurav Satpathy “photovoltaic power control using mppt and boost converter”

Department of Electrical Engineering National Institute of Technology, Rourkela 2012

[13]. Aissa Kheldoun “Mathematical model of the solar system “Renewable Energy lecture notes, IGEE, Boumerdes, 2019

[14]. Hairul Nissah Zainudin, Saad Mekhilef, “Comparison Study of Maximum Power Point Tracker Techniques for PV Systems”, Cairo University, Egypt, December 19-21, 2010, Paper ID 278.

[15]. Katherine A. Kim and Philip T. Krein, “Photovoltaic Converter Module Configurations for Maximum Power Point Operation”, University of Illinois Urbana-Champaign Urbana, PhD thesis, IL 61801 USA.

[16]. Dhananjay Choudhary and Anmol Ratna Saxena, “DC-DC Buck Converter for MPPT of PV System”, International Journal of Emerging Technology and Advanced Engineering (IJETA), vol. 4, no.7, July 2014, 813-821.

[17]. M.A. Farahat, H.M.B. Metwally, Ahmed Abd-Elfatah Mohamed, “Optimal choice and design of different topologies of DC-DC converter used in PV system, at different climate conditions in Egypt”, Renewable Energy, Vol., no., 43, 2012 393,402.

[18]. M. Yunliang, G. Meifeng, and Z. Chaochao, “Research of PV MPPT control strategy based on particle swarm optimization,” Manufacturing Automation J-Global, vol. 37, pp. 52-54, July 2015.

[19]. Ehtisham Lodhi, Rana Noman Shafqat, and Kerrouche K. D. E ”Application of Particle Swarm Optimization for Extracting Global Maximum Power Point in PV System under Partial Shadow Conditions”, BeiHang University, Beijing, China 2012

[20]. Kashif Ishaque, Zainal Salam, Muhammad Amjad, Saad Mekhilef “An Improved Particle Swarm Optimization (PSO)–Based MPPT for PV With Reduced Steady-State Oscillation”. In proceedings IEEE Transaction on power electronics, VOL. 27, NO. 8, AUGUST 2012.

[21]. MAALLEM Yahya, GHEDJATI Karim Eddine, ” Maximum Power Point Tracking (MPPT) for PV system using Exchange Market Algorithm with partial shading capability”, Institute of Electrical and Electronic Engineering, 2018.

[22]. Aissa Kheldoun, Rafik Bradai, Rachid Boukenaoui, Adel Mellit “A new golden section method based MPPT algorithm for photovoltaic systems”, Energy Conversion and Management, 111, 125-136, 2016.

University M'Hamed
BOUGARA - Boumerdes

Institute of Electrical and
Electronic Engineering



Department of Power
and Control

Authorization for Final Year Project Defense

Academic year: 2018/2019

The undersigned supervisor: Prof. Aïsse Khelilany
authorizes the student(s):

Zerrouti Nihal Option: Power Eng.
Dahman Ghennima Option: Power Eng.
/ Option: /

to defend his/ her / their final year Master programme project entitled:

Control of Stand-alone PV-system Under
Non-Uniform Irradiance

during the ☒ June ☐ September session.

Date: 20/06/2019

The Supervisor

The Department Head

Prof. Aïsse Khelilany
[Signature]

